ELSEVIER

Journal of Molecular Structure 599 (2001) 381–425

Journal of
MOLECULAR
STRUCTURE

www.elsevier.com/locate/molstruc

Analytical three-body interaction potentials and hydrogen bond dynamics of hydrogen fluoride aggregates, $(HF)_n$, $n \geq 3$ ☆

Martin Quack[a,*], Jürgen Stohner[a], Martin A. Suhm[b]

[a] *Laboratorium für Physikalische Chemie der ETH Zürich (Hönggerberg), CH-8093 Zürich, Switzerland*
[b] *Institut für Physikalische Chemie, Universität Göttingen, Tammannstr. 6, D-37077 Göttingen, Germany*

Received 5 February 2001; accepted 29 June 2001

Abstract

Oligomeric aggregates of hydrogen fluoride are important prototype molecules for a detailed understanding of the structure, energetics, spectroscopy and dynamics of hydrogen bonding. The pairwise additive description of these oligomers is known to be inadequate. We have sampled the three-body potential for HF at 3000 $(HF)_3$ configurations selected by various classical and quantum sampling techniques, including dynamic sampling based on Voronoi step representation. The counterpoise-corrected Møller-Plesset second-order three-body energies using a double zeta Gaussian basis set with polarization functions (DZP + MP2) at these configurations are fitted by analytical 12-dimensional potentials. Cooperative effects are found to be sizeable and predominantly stabilizing in hydrogen fluoride ring aggregates. Test calculations with larger basis sets and for larger HF aggregates show that in combination with available high quality pair potentials, the analytical three-body terms give an excellent description of the $(HF)_3$ surface in the hydrogen bonding region and a good approximation for clusters up to at least the hexamer. Multidimensional vibrational quantum Monte Carlo calculations indicate that degenerate HF stretch excitation in $(HF)_3$ (3712 cm^{-1}) is in close coincidence with $(HF)_3 \rightarrow 3HF$ dissociation channels at low HF angular momentum, whereas degenerate DF stretch excitation in $(DF)_3$ (2725 cm^{-1}) falls slightly below any $(DF)_3 \rightarrow (DF)_2$ + DF dissociation channels. The $(HF)_3$ potential surface, its stationary points, possible interconversion tunneling pathways, zero point energies, adiabatic channels, unusual isotope effects, fully centrifugal rotational states and the harmonic infrared spectrum are discussed in detail and compared to ab initio calculations and experiment. The applicability of the (1 + 2 + 3)-body approach for larger oligomers ($3 < n < 8$) is investigated with special emphasis on structure, energetics, infrared and microwave spectra, and predissociation. Neglect of four- and higher-body contributions and hydrogen exchange symmetry is found to affect some properties significantly, but the preference for simple ring structures remains pronounced.

Keywords: Hydrogen fluoride trimer; Hydrogen bond; Potential hypersurfaces; Infrared spectra; Quantum Monte Carlo

1. Introduction

High resolution spectroscopic investigations have contributed fundamentally to our understanding of the weak binding and interaction potentials of closed shell molecules (see Refs. [1–5] for just a few outstanding examples from microwave spectroscopy). Hydrogen fluoride clusters and in particular $(HF)_2$ have played an important role in this context as prototypes for

☆ This paper is dedicated to Professor Alfred Bauder in appreciation of his significant contributions to the field of microwave spectroscopy.

* Corresponding author. Tel.: +41-1-632-4421; fax: +41-1-632-1021.

E-mail addresses: martin@quack.ch (M. Quack), msuhm@gwdg.de (M.A. Suhm).

0022-2860/01/$ - see front matter
PII: S0022-2860(01)00825-0

hydrogen bonding from the very start of this field, beginning again with microwave spectra [6], continued by mid-infrared spectra [7–12], far-infrared spectra [13–17] and finally near-infrared spectra [18–23]. Such investigations continue to flourish including higher clusters [24,25] and the references given provide only examples, with fairly complete reviews being available for the (HF)-cluster work [26,27]. Among the most important applications of this wealth of accurate spectroscopic data one can certainly name the constraints placed on possible formulations of potential energy hypersurfaces characterizing the various interactions between the monomers bound together in these clusters. Such interactions are at the heart of the vast and quickly developing fields of molecular recognition and 'supramolecular chemistry' as well as of the transition from the chemistry of quasi isolated molecules in the gas phase to the chemistry of condensed phases.

While many investigations of the structure and dynamics of molecular clusters and condensed matter are still based on pairwise interactions between the constituents, the potential importance of irreducible three- and higher-body contributions for many properties and classes of substances has been known for a long time [28–34] and is currently being elucidated by spectroscopic and theoretical techniques [35–48]. Historically, the long-range Axilrod–Teller or triple-dipole dispersion term [49] for non-polar species at long range is among the most systematically studied three-body interactions, mainly because of the relatively high accuracy of available rare-gas pair potentials. In practice, however, three body interactions play a much more significant role in the intermediate and short range potential of ionic and highly polar substances [50–52]. The cooperative phenomena observed in hydrogen bonded networks suggest particularly pronounced effects [38,53–58]. Hydrogen fluoride is therefore a well-suited model candidate for the systematic study of non-pairwise interactions, although the water system has received considerably more attention, due to its omnipresence.

The fundamental prerequisite for the study of non-pairwise forces between molecules is a detailed knowledge of the *pair* potential. For properly defined molecular boundaries, this is the dominant contribution to the overall interaction energy. Accurate pair potentials are only recently becoming available for hydrogen bonded systems in general and for the simplest prototype HF in particular [59–64]. These 'true' pair potentials, which are obtained from experimental dimer data and ab initio calculations, should be distinguished from effective pair potentials [65,66], which have been very popular in the simulation of liquids and which try to mimic many-body interactions by modified pair interactions, based on adjustment to experimental bulk phase data. Whenever nonadditive interactions are significant, such effective approaches may fail outside the property range to which they have been adjusted. For example, they predict the wrong binding energy for dimers, where molecular many-body interactions are absent by definition.

A successful way for introducing important three- and higher body contributions to the energy of polar systems is via polarization terms [38,51,67–70]. Such self consistent polarizable models contain usually only a few adjustable parameters (the polarizability α and perhaps its anisotropy) and appear to work well where second and higher order induction is the dominant three-body contribution (such as in liquid HCl [68,71]), although they can be computationally quite demanding in terms of CPU time and memory. However, for first row hydride aggregates the situation is probably more complex. While classical polarization is an important and for large distances the dominant three-body contribution, other non-additive effects such as restrictions from the Pauli exclusion principle to polarization and more general exchange interactions come into play [72,73] at the short and intermediate distances relevant for the hydrogen bond dynamics in clusters and liquids. For the water system, ab initio calculations have been used in a systematic way to check and improve the range of applicability of simple three-body potentials for quite some time. The finding was that a simple first order polarization model based on atomic charges could reproduce ab initio three-body energies at long and intermediate water–water distances reasonably well, *once* some adjustments in functional form and polarizability parameters were applied [53,74,75]. It is now clear that such a model is too simple near equilibrium [73,76], whereas more refined treatments of the polarization effects have been quite successful [69,77].

The goal of our investigations is to obtain a three-body potential energy hypersurface for hydrogen fluoride with an accuracy that is useful for spectroscopy, kinetics and thermochemistry of hydrogen fluoride clusters. Based on the continuously

improving and now very accurate monomer and pair potential for this prototype system [59–63], such a three-body potential can be rigorously tested by comparison with experimental data for HF trimer. The appropriate ab initio methods are well established [73,78–81] including studies of the HF trimer [78,81]. The study in Ref. [78] provides decomposed energies for 10 exploratory $(HF)_3$ configurations and firmly establishes a striking insensitivity of the ab initio three-body energy to basis size, correlation level and to some extent even basis set superposition error (BSSE) [33]. These findings, confirmed in the present work, are extremely encouraging for the task of scanning the 12-dimensional three-body surface of the 30 electron system $(HF)_3$. The configurational scanning technique in high dimensional space deserves careful consideration. A systematic grid scan is not practical. In view of our purpose to study the quantum hydrogen bond dynamics in HF clusters and ultimately in condensed phases, iterative scanning strategies based on diffusion quantum Monte Carlo and other Monte Carlo methods were employed and found to be very useful. They are described together with the electronic ab initio approach and analytical representations in Section 3. Analytical formulations can be both tedious and biased for multidimensional potential energy hypersurfaces. An alternative representation based on Voronoi polyhedra built around discrete configurations [82,83] turns out to be helpful in this context and is also outlined in Section 3.

The most immediate application of an analytical or Voronoi-represented three-body potential of HF is to calculate the structural properties and fully anharmonic vibrational dynamics of $(HF)_3$ (Section 4) and higher oligomers (Section 5). Comparison with available harmonic vibrational frequencies from ab initio calculations [78,79,81,84–89], with the vibrational dynamics in empirical potentials [35,38,89–92] and with the growing experimental information on HF trimer and oligomers (Refs. [26,27] and references cited therein) will be possible. Examination of the many-body expansion convergence for HF clusters and of the analytical potential representations will show whether reliable applications to the structure and dynamics of liquid, solid and supercritical HF [38,65,93–101] are already in sight. A preliminary account of the present theoretical investigations has been given at the 1992 EUCMOS 21 conference [102]. Some key results have been used and referred to in Refs. [26,27,103–106]. Several predictions have already triggered experimental progress for the trimer species [107,108] and for higher oligomers [109–111]. A recent, brilliant experimental investigation [25] supports the assignments proposed in Refs. [109–111], thus providing evidence for the usefulness of these potentials for spectroscopy. An important motivation for the present paper is to make the derived analytical three-body potential energy surfaces generally available (see Appendix A).

2. *n*-Body decomposition of hydrogen fluoride potentials

We partition the potential energy $V_{i,i_2\cdots i_n}$ of a system consisting of n particles (in this case HF monomers, note that the concept often refers to atomic fragments, instead [112,113]) with indices i_k $(k = 1, 2, \ldots, n)$ into a sum of m-body contributions $(0 < m \leq n)$ $V^m_{j_1 j_2 \cdots j_m}$ from m-tuples $\{j_k\}$, which form an ordered subset of $\{i_k\}$:

$$V_{i_1 i_2 \ldots i_n} = V^n_{i_1 i_2 \ldots i_n} + \sum_{k=1}^{n} V^{n-1}_{i_1 i_2 \ldots i_{k-1} i_{k+1} \ldots i_n} + \sum_{k=1}^{n} \sum_{l=2\ l>k}^{n} V^{n-2}_{i_1 i_2 \ldots i_{k-1} i_{k+1} \ldots i_{l-1} i_{l+1} \ldots i_n} + \cdots + \sum_{k=1}^{n} V^1_{i_k} \tag{1}$$

This is done in the hope that the contribution of m-body terms to the total energy drops sharply with increasing m for physically reasonable geometries, i.e. the many-body expansion converges rapidly. An m-body term definition which is consistent with the above partition scheme is:

$$V^m_{j_1 j_2 \ldots j_m} = V_{j_1 j_2 \ldots j_m} + (-1)^1 \sum_{k=1}^{m} V_{j_1 j_2 \ldots j_{k-1} j_{k+1} \ldots j_m} + (-1)^2 \sum_{k=1}^{m} \sum_{l=2\ l>k}^{m} V_{j_1 j_2 \ldots j_{k-1} j_{k+1} \ldots j_{l-1} j_{l+1} \ldots j_m} + \cdots + (-1)^{m-1} \sum_{k=1}^{m} V^1_{j_k} \tag{2}$$

In particular, one obtains the conventional two-body (pair potential) and three-body terms (m in V^m is used here as an extra upper index, not an exponent for power):

$$V_{12}^2 = V_{12} - V_1 - V_2 \tag{3}$$

$$V_{123}^3 = V_{123} - V_{23} - V_{13} - V_{12} + V_3 + V_2 + V_1 \tag{4}$$

Higher terms can also be computed recursively using Eq. (1). Note that $V^m_{j_1 j_2 \cdots j_m}$ has to vanish for configurations in which at least one of the monomers j_k is completely separated from the others. For a given m-body term, a total of $2^m - 1$ ab initio calculations have to be performed at each configuration, if symmetry does not make some of the contributions equal. In order to compensate in a consistent way for the basis set superposition error (BSSE) using the counterpoise method [114], all these calculations have to be carried out in the full basis of the m-body system, even though $2^m - 2$ only involve a subset of the m particles. Thus, the computational effort grows exponentially with m. This may raise doubts about advantages of the m-body expansion over a direct approach, which needs one calculation without, or $m + 1$ calculations with counterpoise correction for each configuration. We want to illustrate such advantages for the case of the three-body HF potential, although they remain valid for the next few higher-body terms, provided they contribute significantly to the dynamics of HF-oligomers (see also Section 5).

Depending on the symmetry of an HF trimer configuration, 3–7 ab initio calculations of trimer basis set size are needed to obtain the three-body term. As discussed in detail in Ref. [78] and confirmed here (see Section 3), the electronic interactions which contribute to this three-body term are much less basis set and correlation dependent than the two- and one-body interactions. An apparently strong correlation dependence of three- and four-body terms in the related water clusters [76] is mostly a consequence of comparing different stationary point geometries. Electron correlation enhances the two-body attraction. This leads to a contraction of the cluster minimum geometry, where three- and higher-body terms are larger. Since the one- and two-body interactions have already been characterized at high levels of ab initio theory [59,63] and have been refined empirically using the large body of experimental information on HF monomer and dimer [61,63], it would be wasteful (and very difficult) to perform systematic full $(HF)_3$ calculations whose one- and two-body components approach the available potentials in quality. This conclusion remains valid in spite of the up to sevenfold effort for the evaluation of a counterpoise corrected three-body energy versus a simple trimer energy, even when we include correlation at the MP2 level and use a DZP basis set for safety at configurations far away from equilibrium, where no systematic tests of correlation and basis set dependence have been reported in the literature, so far.

A further advantage of the many-body expansion relates to the analytical fitting procedure, which is a critical and certainly the most laborious step in high dimensional configuration space. By partitioning the potential into terms which anticorrelate importance and dimensionality, as in the many-body expansion of well behaved molecular aggregates, a minimum of fitting effort and bias is achieved. Furthermore, the resulting 'portability' of the separate terms makes further improvements easier to incorporate. A potential disadvantage of such a portable partitioning scheme should be mentioned: The severe problem of fitting artifacts ('holes') becomes harder to diagnose, since an apparent hole in the m-body term may in fact be no artifact at all in the full potential via compensation by k-body terms with $k < m$. However, careful analytical design and configuration sampling can reduce this problem considerably.

Convergence and modularity of the truncated n-body expansion, favourable ab initio aspects of the three-body term for polar systems and iterative stochastic quantum sampling of the multidimensional configuration space are the three principles on which our procedure is based. These principles are fairly general and can be applied to other cooperative systems. The following sections describe the details of an application to HF clusters. Here, the effects are pronounced and the available experimental data base can be used to explore the strengths and limitations of the approach and its analytical parameterization.

3. Computational details and analytical potential surfaces

3.1. Ab initio calculations

Electronic calculations, mostly at the correlated level of second order Møller-Plesset perturbation theory (MP2) have largely been performed with the Cray version of CADPAC [115] and with a DEC Alpha workstation implementation of GAUSSIAN 92 [116]. In order to select a suitable basis set, we have performed a number of test calculations on monomer, dimer and trimer properties. The largest basis used consists of 53 basis functions per monomer subunit. For hydrogen, we used (10s3p) contracted to [6s3p], and for fluorine we used (13s8p2d) contracted to [8s6p2d] [117,118]. This basis gives good results for most HF monomer properties, but the perpendicular polarizability component is somewhat too small ($\alpha_\perp = 3.7(4\pi\epsilon_0 a_0^3)$), also compared to other large basis sets employed [59,79]. Geometries of all stationary points were fully optimized, harmonic vibrational frequencies and intensities have been determined at the MP2 level.

Counterpoise (CP) correction of *optimized* stationary point energies is less straightforward than for the *m*-body decomposition scheme [119]. We include monomer relaxation (MR) contributions [120] and in some cases we reoptimize the structure on the BSSE-corrected surface to avoid overcorrection. For the basis sizes employed in this work, BSSE-correction is likely to lead to underestimated binding energies, since only a fraction of the correlation energy is recovered. Uncorrected binding energies thus profit from error compensation. In Ref. [102], the monomer relaxation term was subtracted from, rather than added to the BSSE, thus also leading to partial error compensation. Scaling to experimental results for a given cluster size can also be helpful in reducing errors due to insufficient basis size or electron correlation treatment [88]. Some of these methods are described and used in Section 4. We emphasize that the *m*-body decomposition scheme advocated in this work solves the BSSE problem in the pair potential via empirical refinement of the ab initio data, while the small BSSE in the three-body potential appears mostly at the SCF level and is eliminated by straightforward CP correction.

While the [8s6p2d/6s3p] basis described above may serve for benchmark comparisons, it is neither practical nor necessary [78] for the scanning of the 12-dimensional three-body contribution (V_R^3) to the potential energy surface of the trimer and higher oligomers, as outlined in Section 2. The three-body energies used in the analytical representation have been calculated using a double zeta plus polarization basis (DZP; $\alpha_p(H) = 1.0$, $\alpha_d(F) = 1.2$) [117,118] at the MP2 level, which is computationally about thirty times more economic. In our pointwise three-body energy comparison of the DZP basis and larger basis set results, the earlier findings of Ref. [78] have been confirmed, as exemplified in Table 1. In this context, it is important to compare the different approaches at the same geometry rather than at their individual minimized geometries [79], since the three-body term is strongly structure dependent. At a given geometry, basis sets of different size give three-body energies (V_R^3) which differ only slightly (about 20 cm^{-1} close to the minimum) at the counterpoise corrected MP2 level. This is in marked contrast to the situation for one- and in particular for two-body energies. Given the slow convergence of polarizabilities with basis set size, this result may appear surprising, as induction is an important three-body contribution. However, the relevant quantity for induction forces is the *product* of polarizability and the squared dipole moment (see below), which shows a faster convergence due to partial compensation of errors. Extensive test calculations for V_R^3 including geometries given in Table 1 confirm that for the larger basis sets, counterpoise correction has almost no effect on the three-body energy and MP2 results are quite close to SCF results. For the DZP basis set, counterpoise corrections are still small, but bring the three-body energy into closer agreement with large basis set results.

While for monomer and dimer properties only the largest basis set calculations proved satisfactory, the DZP basis set is therefore well justified for the separated three-body part of the HF interaction potential. This basis set permits the evaluation of many trimer geometries at the counterpoise corrected MP2 level (DZP + MP2 − BSSE) and also enables the study of three- and more-body effects in much larger HF oligomers.

In order to have an independent estimate for *qualitative* trends in the HF polymerization sequence, we

Table 1
Comparison of values predicated by the analytical HF3BL potential (V^3_{HF3BL}) with the available three body energies (V^3_R) for bonded $(HF)_3$ configurations (all C_{3h}-symmetry and thus characterized by the monomer bond length r_{HF}, the FF-distance R_{FF}, and the angle formed by the FH bond and the line joining the F atoms involved in the hydrogen bond, ∠FFH) from the literature [78,79] and from some of our own larger basis set benchmarks. MPn: n^{th} order Møller-Plesset perturbation theory; S designates a medium-polarized (Sadlej) basis set (see Ref. [78]), whereas VP^s designates a modification of the 6-31G** basis (see Ref. [79]). All results include counterpoise corrections for the BSSE (see also Ref. [105]).

V^3_{HF3BL}/hc (cm^{-1})	V^3_R/hc (cm^{-1})	r_{HF} (pm)	R_{FF} (pm)	∠FFH (deg)	Lit.	Method
−589	−565	91.7	273	26.9	[78]	S + MP3
−214	−191	91.7	273	60.0	[78]	S + MP3
−1277	−1161	91.7	250	26.9	[78]	S + MP3
−27	−28	91.7	400	37.0	[78]	S + MP3
−6	−6	91.7	500	40.6	[78]	S + MP3
−925	−1077	91.3	261	24.1	[79]	6-31G**
−1092	−1140	91.3	256	24.1	[79]	6-31G** + MP2
−590	−581	91.1	272	27.4	[79]	VP^s
−630	−605	91.1	270	27.4	[79]	VP^s + MP2
−1164	−1205	93.3	259	21.4	This work	[5s4p2d/3s2p1d] + MP2
−1058	−1104	93.4	262	21.6	This work	[8s6p2d/6s3p] + MP2
−1058	−1085	93.4	262	21.6	This work	DZP + MP2
−1391	−1371	93.2	250	26.9	This work	[8s6p2d/6s3p] + MP2
−1391	−1387	93.2	250	26.9	This work	DZP + MP2
−1013	−1036	93.2	262	23.6	This work	[8s6p2d/6s3p] + MP2
−1013	−1046	93.2	262	23.6	This work	[5s4p2d/3s2p1d] + MP2
−1013	−1025	93.2	262	23.6	This work	DZP + MP2
−563	−579	90.9	273	26.9	This work	[5s4p2d/3s2p1d] + MP2

have also calculated minimum properties at the DZP + MP2 level for oligomers up to the octamer, including harmonic frequencies up to the heptamer (see Tables 2 and 3). These results may be compared to the more accurate but less complete data in Ref. [88] and to more recent ab initio calculations covering a range of cluster sizes [81,122–124]. While absolute binding energies and frequencies using such a small basis set are necessarily unreliable, size dependent trends are nevertheless extractable. In particular, this independent data set allows for a qualitative judgment of the validity of our analytical potential for oligomers beyond the trimer, as it is not influenced by possible range limitations present in analytical representations. Furthermore, the DZP + MP2 data can be analyzed in detail with respect to BSSE and many-body contributions.

3.2. Quantum sampling of configuration space

The exploration of 12-D configuration space for the three-body potential of HF is by no means trivial if the number of configurations is restricted to some 10^3 due to computational limitations. Any systematic grid strategy is completely impractical and would mostly sample points of little relevance or leave out many of high relevance to the purpose of the investigation — namely the large amplitude intermolecular dynamics of HF clusters. The procedure which we have used to sample the 12-dimensional three body configuration space is thus composed of several steps. In a first stage, a very coarse grid consisting of about 100 C_3-symmetric $(HF)_3$ configurations (which span a 4-D subspace) was calculated and used for a first analysis of the three-body energy and its major contributions. In the second step, about 200 random C_3 configurations within radial bounds of 1.5–2.0a_0 for bonded HF lengths and 4.2–7.0a_0 for HF center of mass distances without orientational constraints for the HF subunits were successively included in the three-body fit until the root mean square (rms) deviation of the employed trial analytical function had converged. This trial function consisted of the leading three-body dipole-induction term augmented by various simple functional forms to mimick the short-range behaviour. The convergence of the fit was taken as an indication

Table 2
Comparison of $(HF)_n$ ($n = 1$–8) minimum geometries, well depths (D_e/kJ mol^{-1}) and *harmonic* estimates (including all degrees of freedom with positive curvature) of the total binding energy D_0^h/kJ mol^{-1} with respect to total dissociation predicted at the DZP + MP2 level. BSSE corrected well depths are given including monomer relaxation (BSSE + MR). In order to assess the overshooting of a posteriori BSSE corrections, we have minimized some smaller clusters on the BSSE-corrected DZP + MP2 surface. The results are given in parentheses. Results in square brackets were obtained by minimizing the DZP + MP2 *pairwise additive* energy only, assuming C_{nh} symmetry (probably not the most stable structure for pairwise additive $(HF)_5$). For $n = 6$, the data for the S_6 chair minimum and for the C_2 twist (t) and C_2 boat (b) stationary points are given together with those for the C_{6h} higher order saddle point. For the chair confirmation, the individual bond lengths and bond angles differ by less than one unit in the last digit quoted; the FFF angle is 115° as compared to the planar angle of 120°. For the twist and boat forms, the FFF angles are between 119 and 120°. The D_4 and S_8 stationary points for $n = 8$ may be saddle points or local minima. The D_4 Structure is a prolate top with $A_e = 0.0331$ cm^{-1} (see also Ref. [105])

n	r_{HF} (pm)	R_{FF} (pm)	∠FFH (deg)	C_e (cm^{-1})	D_e	D_0^h	$D_e^{BSSE+MR}$
1	91.9			20.847	–	–	–
2	92.4, 92.3	274	8.2, 67.3	0.2269	24.1	16.1	18.7
	(92.4, 92.2)	(282)	(5.9, 59.0)				(19.2)
3	93.5	261	23.6	0.1261	78.1	56.2	56.3
	(93.1)	(270)	(25.1)				(57.8)
	[92.2]	[270]	[25.5]		[67.8]		
4	94.5	253	11.5	0.0668	138.8	105.1	106.2
	(93.9)	(261)	(12.8)				(108.2)
	[92.1]	[268]	[13.8]		[108.0]		
5	94.9	250	5.6	0.0378	188.5	145.4	148.1
	(94.2)	(257)	(6.6)				(150.7)
	[92.1]	[269]	[7.8]		[139.2]		
$6^{C_{6h}}$	95.0	249	2.0	0.0229	230.6	179.4	184.1
6^{S_6}	95.0	249	3.5	0.0242	231.3	179.1	
6^{C_2}(t)	95.0	249	2.2–2.4	0.0231	230.6		
6^{C_2}(b)	95.0	249	2.1–2.3	0.0230	230.6		
7^{C_1}	95.0–95.1	248–249	2–3		271.4	211.3	
8^{D_4}	94.4	254	12.5	0.0302	288.6		
8^{S_8}	94.5	251	0.9	0.0106	310.8		

for the saturation of 4-D space with sample points. At this point, sampling of the full 12-D space of $(HF)_3$ set in. We have opted for an iterative stochastic procedure based on the diffusion quantum Monte Carlo (DQMC) method. Rovibrational DQMC is described in detail elsewhere [61,125] and is summarized later in this section. Briefly, the technique generates a discrete weighted distribution proportional to the exact rovibrational ground state wave function for a given potential energy surface. It is thus more appropriate for sampling the configuration range sampled by the light particle (tunneling) dynamics of $(HF)_3$ than a finite temperature classical Metropolis Monte Carlo scheme. To extend the sampling beyond the ground state amplitude, weight selection strategies were employed. Alternatively, one could also simulate $(HF)_3$ using reduced atomic masses [61]. The first 150 DQMC configurations were obtained from a pair potential simulation of $(HF)_3$ using monomer bias and continuous weights, much as described for $(HF)_2$ in Ref. [61], but with a somewhat modified one- and two-body potential (SNC [26,106]). These points were used in the three-body fit without their DQMC weights, thus extending the sampling somewhat beyond the ground state *amplitude* (which in any case extends considerably beyond the ground state *probability*). After some trial fits with different functional forms a preliminary three-body potential was obtained. This was then added to the pair potential in a subsequent DQMC simulation, yielding 100 new and more representative $(HF)_3$ configurations, in addition to a first estimate of the fully anharmonic trimer quantum dissociation energy D_0. This two-step sequence consisting of analytical trial fits and DQMC generation of new configurations using the refined total (1 + 2 + 3)-body potential of $(HF)_3$ was iterated several times. During the process the weight threshold above which the DQMC configurations

Table 3
Comparison of $(HF)_n$ ($n = 3$–6)C_{nh} harmonic (normal mode) wavenumbers ω_e (in cm^{-1}) predicted by the analytical HF3B(L/G) term (added to the empirically refined accurate ab initio pair potentials SQSBDE [61], SNC [26,62,106] and SC − 2.9 [63]) with ab initio results. The harmonic monomer stretching frequencies are given in parentheses in the source column. Infrared-active vibrations (E', A'' or $E_{(1)u}$, A_u) are written in bold face (d = degenerate (E), i = imaginary, ip = in plane, op = out of plane, str. = stretch, def. = deformation). The op/ip classification for the S_6 vibrations is somewhat arbitrary and based on correlations with the C_{6h} vibrations. Included are predictions by the MMC model [121] for $n = 3$. Within the MMC framework, 3-D subspace anharmonic results have been obtained [35] for $(HF)_3$ and are also given. Predictions by a recent DIIS model [89] are included for $n = 3, 5$

n	HF str.	ip bend	ip str.	ip def.	op bend	op def.	Source
3	**3884d**	980	**209d**		**719**		HF3BG + SC-2.9 pair potential
	3807	**625d**	228		500d		(4134)
	3994d	822	**149d**		**592**		SC-2.9 pair potential only
	3960	**454d**	201		382d		(4134)
	3950d	844	**181d**		**621**		HF3BL + SNC pair potential
	3792	**510d**	180		421d		(4133)
	4055d	725	**129d**		**522**		SNC pair potential only
	3979	**376d**	173		331d		(4133)
	3885d	854	**184d**		**625**		HF3BL + SQSBDE pair potential
	3822	**527d**	182		425d		(4138)
	3868d	876	**184d**		**639**		HF3BG + SQSBDE pair potential
	3820	**549d**	193		448d		(4138)
	3904d	989	**205d**		**726**		[5s4p2d/3s2p1d] + MP2 (this work)
	3779	**626d**	225		516d		(4198)
	3974d	986	**203d**		**722**		DZP + MP2 (this work)
	3862	**598d**	228		494d		(4221)
	3964d	923	**191d**		**672**		ACPF [88]
	3863	**562d**	208		486d		(4182)
		1016	**117d**		**629**		MMC [121]
		599d	240		406d		
		801			**568**		Electrical potential [35]
		491d			376		anharmonic, ip–op–radial separation
	3938d	1001	**163d**		**581**		DIIS [89]
	3843	**586d**	183		361d		
4	3839	1018	296	83	**770**	41	HF3BG + SC-2.9 pair potential
	3747d	**777d**	**275d**		636d		
	3637	657	208		573		
	3904	848	225	75	**623**	41	HF3BL + SNC pair potential
	3892d	**632d**	**214d**		500d		
	3718	528	167		454		
	4075	765	176	51	**538**	14	SNC pair potential only
	4017d	**539d**	**176d**		413d		
	3950	429	165		378		
	3691d	970	306	99	**723**	46	HF3BG + SQSBDE pair potential
	3781	**742d**	**281d**		599d		
	3587	657	210		557		

Table 3 (*continued*)

n	HF str.	ip bend	ip str.	ip def.	op bend	op def.	Source
	3827	1150	296	93	**829**	46	DZP + MP2
	3749d	**877d**	**281d**		693d		this work
	3562	673	219		631		
	3836	1120	300	90	845	47	ACPF [88]
	3757d	**870d**	**282d**		718d		
	3571	700	213		647		
5	3830d	961	337d	67d	**730**	25d	HF3BG + SC-2.9 pair potential
	3716d	**801d**	**252d**		650d		
	3629	656d	178		598d		
	3924d	804	244d	49d	**576**	26d	HF3BL + SNC pair potential
	3872d	**647d**	**195d**		499d		
	3745	540d	138		466d		
	3710d	929	371d	62d	**693**	25d	HF3BG + SQSBDE pair potential
	3832d	**767d**	**279d**		614d		
	3622	664d	195		580d		
	3746d	1183	361d	80d	**837**	23d	DZP + MP2
	3622d	**989d**	**278d**		755d		this work
	3425	767d	190		718d		
	3848d	1045	302d	78d	**626**	18d	DIIS [89]
	3728d	**861d**	**237d**		543d		
	3528	605d	149		465d		
6	3869	877	407	88	**661**	25	HF3BG + SQSBDE pair potential
C_{6h}	3817d	**763d**	362d	48d	607d	**15d**	this work
	3705d	664d	**241d**		585d		
	3639	623	166		581		
C_{6h}	3754	1155	404	101	**813**	24i	DZP + MP2
	3711d	**1015d**	361d	58d	759d	8id	this work
	3571d	835d	**249d**		741d		
	3396	741	162		744		
S_6	**3747**	1137	**394**	**91**	**899**	41	DZP + MP2
	3701d	**1016d**	355d	53d	753d	**27d**	this work
	3561d	896d	**256d**		**737d**		
	3387	**736**	175		728		

are discarded was gradually lowered in order to sample more of the relevant higher energy configuration space. After the collection of about 900 configurations, convergence and space saturation appeared sufficient for the hydrogen bond dynamics of $(HF)_3$ and a final effort was put into the refinement of the analytical potential. For this step, another 100 configurations close to the $(HF)_3$ minimum structure were generated, bringing the total number of three-body energies to 1004 (from 5352 trimer basis set calculations). The three-body energies were weighted according to their associated full ab initio $(HF)_3$ energy, since that quantity correlates with their relative importance for the $(HF)_3$ hydrogen bond dynamics. The 335 configurations up to 5000 cm^{-1} above the minimum were given unit weight, the higher energy weighting sequence was 0.3/0.1/0.03/0.01/0.003/0.001 in bins of 5000 cm^{-1} (>30000 cm^{-1}

for the 0.001-weights) with 438/159/43/15/9/5 configurations per bin. This sampling and weighting scheme concentrates on the description of three-body interactions in the *trimer* hydrogen bonding region.

3.3. Description of the HF3BL analytical potential

Several criteria for the analytical three-body potential were defined at the outset of the fitting procedure:

1. The leading term at long distances, in this case the second order dipole induction contribution, is fixed using known experimental values for the dipole polarizability, its anisotropy and the dipole moment of HF. Compared to distributed charges [53,126], a point dipole formulation is more compatible with the available pair potentials.
2. No attempt is made to include higher order induction terms (neither in the multipoles nor in the polarizability) in a similar way due to the poor convergence of the multipole expansion at short and intermediate distances and the importance of exchange repulsion. Selection of the functional form in this region is governed mostly by the fit quality.
3. Singularities in the analytical potential are restricted to configurations with superimposed atoms or HF centers of mass in order to reduce the chance of artifacts in physically relevant regions of the configuration space.
4. The computational effort required for the evaluation of the three-body term should not be larger than that of the available pair potential code, which in turn has been carefully optimized for maximum performance on vector computers (e.g. 0.7 μs at 2.3 Gflop/s on one processor of the NEC SX-3/24R for one of 1024 simultaneous potential evaluations). This ensures that the three-body part accounts for less than 50% of the computational effort up to medium-size clusters. For larger clusters, cutoff methods may be used to avoid a three-body overhead, since the two-body forces have a longer range.
5. The maximum acceptable rms deviation of a properly weighted fit of the potential to the ab initio three-body energies is about $100\,cm^{-1}$, since the absolute error of the ab initio approach for the three-body energies is estimated to be less than $100\,cm^{-1}$ for most of the relevant configurations. In addition, the three dimer interactions occurring in $(HF)_3$ currently also have a cumulated fitting uncertainty of somewhat less than $100\,cm^{-1}$ [61,63].
6. No Axilrod-Teller type triple-dipole dispersion term is included in the fit, since this term only appears at the MP3 level (dispersion interactions are additive at the MP2 level [78]) and was shown to be negligible for the relevant $(HF)_3$ configurations [78].
7. The three-body potential is required to have the full permutation inversion symmetry with respect to exchange of the HF units, as in the case of the analogous two-body potentials [61,63]. No hydrogen exchange symmetry is currently built in, although the corresponding transition state for $(HF)_3$ lies lower than in $(HF)_2$ at about 85(10) kJ mol^{-1} [105,119]. This limits the validity of the three-body potential to FF distances above $\approx 4.2a_0$. It also prevents us from applying the surface to reactive processes with H-exchange, which are of interest also in relation to detailed symmetry selection rules [127]. Generalizations to include these effects have been discussed in Refs. [26,27].

The coordinates used in our analytical representation of the HF three-body potential are defined in Fig.,1 in terms of the three hydrogen sites and the three HF centers of mass. s_{jk} and t_{jk} denote the three center–center and hydrogen–hydrogen distances, respectively. The r_{jk} represent the nine mixed center-hydrogen distances, of which the three r_{jj} are proportional to the monomer bond lengths. The unit vectors $\vec{e}_i$ and $\vec{e}_{ij}$ along the monomer HF bonds and the center–center lines are used to define four different types of angle cosine:

$$\vec{e}_i \cdot \vec{e}_j = \cos\alpha_{ij} \quad \text{with} \quad i \neq j,\ \cos\alpha_{ij} = \cos\alpha_{ji} \tag{5}$$

$$\vec{e}_{ij} \cdot \vec{e}_{kj} = \cos\beta^j_{ik} \ \text{with}\ i \neq j \neq k \neq i,\ \cos\beta^j_{ik} = \cos\beta^j_{ki} \tag{6}$$

$$\vec{e}_k \cdot \vec{e}_{ij} = \cos\gamma^k_{ij} \ \text{with}\ i \neq j \neq k \neq i,\ \cos\gamma^k_{ij} = -\cos\gamma^k_{ji} \tag{7}$$

$$\vec{e}_i \cdot \vec{e}_{ij} = \cos\theta_{ij} \quad \text{with} \quad i \neq j. \tag{8}$$

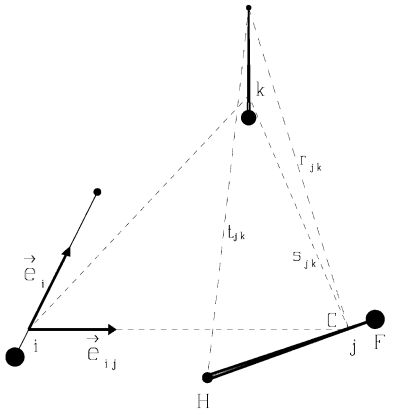

Fig. 1. Definition of internal coordinates used for the analytical representation of the HF3BL three-body potential. i, j, k represent three interacting HF monomers with corresponding centers of mass C (as obtained for $m_H = 1.007825$ u and $m_F = 18.9984$ u). r_{jk} is the distance between the center of molecule j and the hydrogen atom of molecule k, hence $r_{jj}(m_H + m_F)/m_F$ is the bond length of molecule j. s_{jk} is the center of mass distance for molecules j and k, thus $s_{jk} = s_{kj}$. t_{jk} denotes the distance between hydrogen atoms of molecules j and k ($t_{jk} = t_{kj}$). $\vec{e}_i$ and $\vec{e}_{ij}$ are unit vectors along the HF molecule i (pointing towards the hydrogen atom) and from the center of i to the center of j, respectively. They are the building blocks of the angles α, β, γ and θ defined in the text. For the HF3BG potential, the centers C coincide with the F atoms, see text.

For the leading three-body term at long distances, we start with the second order dipole induction term for an n-particle system [74,75]:

$$V_{\text{ind}} = -\tfrac{1}{2}\sum_{j=1}^{n}[\alpha_{\perp j}(\vec{\mathscr{E}}_j\cdot\vec{\mathscr{E}}_j) + (\alpha_{\|j} - \alpha_{\perp j})(\vec{\mathscr{E}}_j\cdot\vec{e}_j)^2] \quad (9)$$

Here, $\alpha_{\perp j}$ and $\alpha_{\|j}$ are the perpendicular (degenerate) and parallel components of the dipole polarizability tensor of molecule j. They are given the values $5.2(4\pi\epsilon_0 a_0^3)$ and $6.6(4\pi\epsilon_0 a_0^3)$, respectively ($1a_0 = 52.9177249$pm), consistent with the available body of experimental data [128,129] and recent ab initio calculations [130]. $\vec{\mathscr{E}}_j$ is the total electrical field at the jth center resulting from the contributions $\vec{\mathscr{E}}_{jk}$ of the dipoles at the centers k:

$$\vec{\mathscr{E}}_j = \sum_{k=1,k\neq j}^{n}\vec{\mathscr{E}}_{jk} \quad (10)$$

By subtracting those components which only depend on two of the interaction centers, we are left with the three-body contribution to V_{ind}:

$$V_{\text{ind}}^{3B} = -\sum_j\left\{\alpha_{\perp j}\left[\sum_{k\neq j}\sum_{l>k,l\neq j}\vec{\mathscr{E}}_{jk}\cdot\vec{\mathscr{E}}_{jl}\right] + (\alpha_{\|j} - a_{\perp j})\left[\sum_{k\neq j}\sum_{l>k,l\neq j}(\vec{\mathscr{E}}_{jk}\cdot\vec{e}_j)(\vec{\mathscr{E}}_{jl}\cdot\vec{e}_j)\right]\right\} \quad (11)$$

where the sums go from 1 to n with the indicated constraints. One can also use the sum equivalence

$$\sum_{j=1}^{n}\sum_{k\neq j}\sum_{l>k,l\neq j}f(j,k,l) = \sum_{j=1}^{n}\sum_{k>j}\sum_{l>k}\{f(j,k,l) + f(l,j,k) + f(k,j,l)\}. \quad (12)$$

For the dipole field contributions $\vec{\mathscr{E}}_{ji}$ from particles i at the site of particle j we have:

$$\vec{\mathscr{E}}_{ji} = \frac{\mu_i(r_{ii})}{4\pi\epsilon_0 s_{ij}^3}(\vec{e}_i - 3\vec{e}_{ij}(\vec{e}_i\cdot\vec{e}_{ij})) \quad (13)$$

where for generality we have included a dependence of the HF dipole moment μ_i on the HF bond length (or rather on the proportional quantity r_{ii}). The simple expression

$$\mu_i/D = \frac{1.11 r_{ii}/a_0}{(r_{ii}/(4a_0))^4 + 1}\, g(r_{ii}, 2a_0) \quad (14)$$

with the switching function

$$g(r,c) = \begin{cases} e^{-\left(\frac{(r-c)}{c}\right)^2} & \text{if } r > c \\ 1 & \text{otherwise} \end{cases} \quad (15)$$

($1\text{ D} = 3.335\,64\times10^{-30}$C m) has the correct limits for $r_{ii}\to 0$ and $\to\infty$ and gives satisfactory values for the dipole moment of HF in between, particularly in the vicinity of the equilibrium value of r_{ii}. Much more accurate HF dipole moment functions are available [131], but are unnecessary for the present purpose. A similar dependence could also be introduced for $\alpha_\perp$ and $\alpha_\|$, but we have not included it at the present stage due to the limited experimental data.

Substitution of the cosine expressions yields:

$$\vec{\mathscr{E}}_{jk}\cdot\vec{\mathscr{E}}_{jl} = \frac{\mu_k(r_{kk})\mu_l(r_{ll})}{(4\pi\epsilon_0)^2 s_{kj}^3 s_{lj}^3}(\cos\alpha_{kl} - 3\cos\gamma_{kj}^{l}\cos\theta_{kj} - 3\cos\gamma_{lj}^{k}\cos\theta_{lj} + 9\cos\beta_{kl}^{j}\cos\theta_{kj}\cos\theta_{lj}) \quad (16)$$

$$(\vec{\mathscr{E}}_{jk}\cdot\vec{e}_j)(\vec{\mathscr{E}}_{jl}\cdot\vec{e}_j) = \frac{\mu_k(r_{kk})\mu_l(r_{ll})}{(4\pi\epsilon_0)^2 s_{kj}^3 s_{lj}^3}(\cos\alpha_{kj}\cos\alpha_{lj} + 3\cos\alpha_{kj}\cos\theta_{jl}\cos\theta_{lj} + 3\cos\alpha_{lj}\cos\theta_{jk}\cos\theta_{kj} + 9\cos\theta_{jl}\cos\theta_{lj}\cos\theta_{jk}\cos\theta_{kj}) \quad (17)$$

This expression does not contain the short-range higher order polarization terms (polarization by induced dipoles, polarization by higher multipoles, etc.). These and all other nonadditive trimer contributions are fitted by two empirically evaluated terms. The first term is an angular expression designed to model short range induction effects:

$$V_1 = -p_1\sum_{j=1}^{n}\sum_{k\neq j}\sum_{l>k,l\neq j}[(\tfrac{1}{4}\cos\beta_{kj}^{l} - \cos\gamma_{kj}^{l}) \times\cos\theta_{kj}(\tfrac{1}{2} + 2\cos\theta_{kj} + 6\cos^2\theta_{kj}) + 3\cos\alpha_{kj}\cos\alpha_{lj} + 2\cos\theta_{jk}\cos\theta_{jl} - 2\cos\theta_{kj}\cos\theta_{lj} - 1 + (\tfrac{1}{4}\cos\beta_{lj}^{k} - \cos\gamma_{lj}^{k})\cos\theta_{lj}(\tfrac{1}{2} + 2\cos\theta_{lj} + 6\cos^2\theta_{lj})] \times\left[\frac{(r_{kk}g(r_{kk},2a_0)/s_{kj})(r_{ll}g(r_{ll},2a_0)/s_{lj})}{((r_{kk}/4a_0)^4+1)((r_{ll}/4a_0)^4+1)}\right]^4 \times h(s_{kj},4a_0)h(s_{lj},4a_0) \quad (18)$$

with

$$h(s,c) = \begin{cases} e^{-\left(\frac{(c-s)}{s}\right)^2} & \text{if } s < c \\ 1 & \text{otherwise} \end{cases} \quad (19)$$

and $p_1 = (1.8 \pm 0.1)\times 10^5\ \mathrm{cm}^{-1}$ (the error given is 3σ of the fit). The damping terms g, h can be conveniently modified in combination with pair potentials which are not repulsive enough and thus lead to artificial minima which are easily accessible from the physical minimum. In high-dimensional spaces it is difficult to exclude artificial minima completely. However, the aim must be at least to ensure that such minima are isolated from the physical minimum by thermally unsurmountable and quantum-mechanically impenetrable barriers. The DQMC algorithm [61] is a very efficient tool to test this condition in practice and did not reveal artificial minima for the HF3BL potential in combination with the pair potentials SQSBDE [61], SNB and SNC [26,106], which are discussed later on. Here, the damping terms g, h do not affect the quality of the three-body fit to the ab initio data, i.e. they act in a configuration range which anyway is not covered adequately by ab initio points. Actually, the h-term is only effective when $s_{ik} < 4a_0$, i.e. when hydrogen exchange becomes feasible and hence the configurations are outside the validity range of the potential.

The second term consists of a sum of exponentials in s_{ij}, t_{ij} and r_{ij} to mimic exchange interaction:

$$V_2 = p_2\sum_{j=1}^{n}\sum_{k>j}^{n}\sum_{l>k}^{n}\{e^{-d_2(t_{jk}+t_{jl})} + e^{-d_2(t_{jk}+t_{kl})} + e^{-d_2(t_{jl}+t_{kl})} + 100[e^{-d_2(s_{jk}+s_{kl}+s_{lj})+2} - e^{-d_2(r_{jk}+r_{kl}+r_{lj})} - e^{-d_2(r_{jl}+r_{kj}+r_{lk})}]\} \quad (20)$$

with $p_2 = (1.6 \pm 0.1)\times 10^4\ \mathrm{cm}^{-1}$ (3σ error) and $d_2 = 0.8a_0^{-1}$ (held fixed in the fit). The total analytical HF three-body (HF3BL) potential[1] for $(HF)_n$ is thus

$$V_{\mathrm{HF3BL}} = V_{\mathrm{ind}}^{3B} + V_1 + V_2. \quad (21)$$

It has a weighted rms deviation of 62.8 cm^{-1} from the 1004 ab initio data points with two free parameters p_1 and p_2. This increases to 184 or 114 cm^{-1} when p_1 or p_2 is held fixed at 0, respectively. V_{ind}^{3B} alone has a rms deviation of 547 cm^{-1}. As the largest absolute three-body energies covered by the ab initio sampling are below 5000 cm^{-1}, the fit quality remains essentially unaffected by the introduction of upper and lower bounds of $\pm 20000\ \mathrm{cm}^{-1}$ via

$$V_{\mathrm{HF3BL}}/\mathrm{cm}^{-1} = 20000\tanh\frac{(V_{\mathrm{ind}}^{3B} + V_1 + V_2)/\mathrm{cm}^{-1}}{20000}. \quad (22)$$

[1] A FORTRAN 77 source code of the analytical HF3BG three-body potential presented here is given in the Appendix A.

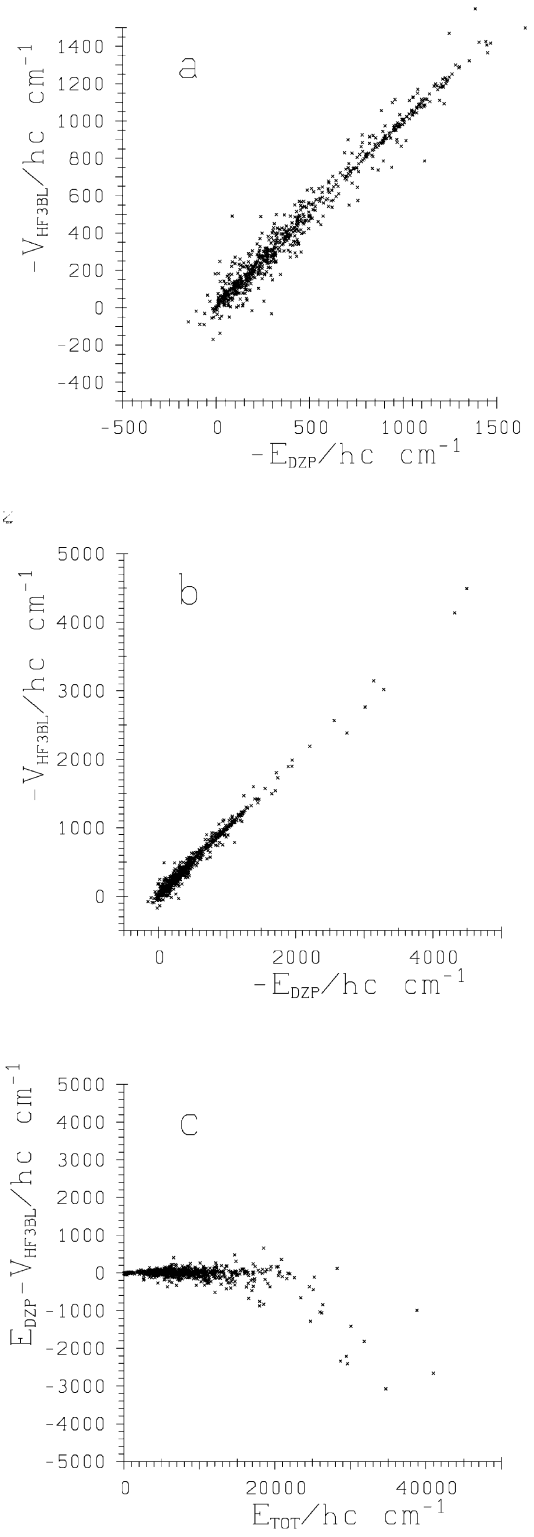

As this function yields additional protection against undesired artificial minima outside the ab initio sampling range, we recommend it in combination with weakly repulsive pair potentials. Fig. 2 gives some insight into the correlations between fitted and ab initio data. In comparing these plots with those available in the literature for the water system [53,54,74], a striking difference can be noted. Whereas in the case of water most of the sampled three-body energies are distributed more or less symmetrically around zero in the range of about 300 cm^{-1}, we find a strongly asymmetric distribution from roughly 100 to -1500 cm^{-1}. Part of this difference is certainly due to the sampling procedure for water, which concentrated more on the long range interactions, while we have sampled more of the rovibrational ground state amplitude of $(HF)_3$. But the discrepancy is also indicative of the more pronounced and systematically *stabilizing* three-body effects in HF ring aggregates.

Table 1 compares available literature values for the three-body contributions of $(HF)_3$ at various bonded geometries and widely different basis sets with the analytical V_{HF3BL} predictions. It demonstrates quite clearly the basis set insensitivity of the investigated quantity as well as the quality of the analytical DZP + MP2 − BSSE fit.

3.4. DQMC calculations in analytical potentials

The Diffusion Quantum Monte Carlo technique (DQMC) [61,132–136] exploits an isomorphism between the *N*-particle time-dependent Schrödinger equation,

$$\frac{\partial \Psi}{\partial(i\cdot t/\hbar)} = \sum_{k=1}^{N} \frac{\hbar^2}{2m_k}\nabla_k^2\Psi - (V - E_0)\Psi \qquad (23)$$

Fig. 2. Correlation plots for the analytical HF3BL fit. (a) Correlation of the analytical HF3BL three-body energy V_{HF3BL} with the ab initio DZP + MP2 three body energy E_{DZP} down to -1500 cm^{-1} for all 669 ab initio points with weights larger than 0.1. (b) As in (a) but for a three-body range down to -5000 cm^{-1}. (c) Correlation of the fit deviations ($E_{DZP}-V_{HF3B}$) with the total DZP $(HF)_3$ energy E_{TOT} counted from the minimum. The systematic deviations for the low weight points beyond $E_{TOT}/hc = 25000$ cm^{-1} help to avoid artificial holes in strongly repulsive ranges, while they are not significant for the hydrogen bond dynamics.

and a 3*N*-dimensional transport equation involving diffusion and reaction for the quantity Ψ

$$\frac{\partial \Psi}{\partial \tau} = \sum_{k=1}^{N} D_k \nabla_k^2 \Psi - k_1 \Psi, \tag{24}$$

when propagated along 'imaginary time' or its reciprocal energy equivalent $\tau = i{\cdot}t/\hbar$. Here, m_k is the mass of the kth particle, V the 3*N*-dimensional potential for the particles and E_0 a so far arbitrary energy offset. D_k describes anisotropic diffusion in 3*N* dimensions and k_1 is a coordinate dependent first order rate constant. Both transport coefficients act on Ψ, which consequently must be a non-negative distribution. The distribution is represented by a discrete, weighted ensemble of points in coordinate space. The reactive and diffusive terms are separated in a short time (Trotter–Suzuki) approximation [132] and can be simulated by weight adjustment and Brownian random motion. The Gaussian pseudo-random numbers required for the latter can now be computed very economically [137] in an approximation which we find perfectly suitable for our DQMC applications. The algorithm is about 6 times faster than previous (already very fast) implementations, also on vector computers, and renders random number generation costs negligible for all but the very simplest interaction potentials. For $\tau \rightarrow \infty$, the simulated Ψ-distribution approaches the (non-negative) wavefunction of the lowest quantum state of the *N*-particle system. E_0, when dynamically adjusted to keep the sum of weights stable, fluctuates around its energy eigenvalue. For pairs or *n*-tuples of identical fermions such as electrons, this state will be Pauli-forbidden and hence not very useful. The lowest physical eigenstate has a wave function with positive and negative lobes and cannot be obtained simply via the diffusion algorithm. Solutions to this so called sign-problem are difficult, but are becoming available (see Ref. [138]).

Given the electronic potential energy hypersurface, DQMC provides an attractive method for the solution of the *internuclear* many-body (i.e. many atom dynamics) problem. Here, the particles are often distinguishable from each other or are *n*-tuples of bosons (such as HF units in $(HF)_n$) and thus have a ground state which is not restricted by the Pauli principle. Even if fermion *n*-tuples cause Pauli restrictions on the total ground state (such as in H_3^+), the boson ground state energy is still useful, as the lowest Pauli-allowed state will be nearby (generally a rotational or tunneling excitation [127]), compared to the dominating effect of vibrational zero point energy. Fundamental advantages of DQMC over basis set methods are the applicability to systems of high dimensionality and the absence of a need for simple zero-order Hamiltonians. This explains the growing interest in quantum Monte Carlo methods for the investigation of zero-point energy effects in multidimensional, anharmonic systems such as van der Waals aggregates (see e.g. Refs. [38,61,69,125,139–141]).

Beyond the powerful application of the method to ground state calculations, which is illustrated in Sections 4 and 5, many extensions to excited states have been investigated (see Refs. [27,61,106,142]). Here we use only two such extensions which have been developed some time ago [61] and shall describe them briefly:

In the clamped coordinate quasiadiabatic channel method, one or more holonomic distance constraints are applied to slow system coordinates (in this case the center of mass distances of HF units), while the zero point energy of the remaining (mostly higher frequency) bath coordinates is simulated. Parametric variation of the constraints generates adiabatic channels [27,61,143,144], which may be interpreted as the best effective reduced-dimensionality potentials for motion in the slow coordinates. This motion, in turn, can then be investigated with standard techniques. Metric tensor effects on the kinetic energy operator due to the introduction of single distance constraints are expected to be small [145]. The quasiadiabatic or Born–Oppenheimer separation in this clamped-coordinate approach averages over *specific* vibrational resonances but describes the important *nonresonant* couplings between stretch and bend modes in hydrogen bonded systems [61], which are largely neglected in a minimum energy path analysis. We may refer here also to the quasiadiabatic channel reaction path treatment of tunneling problems [146,147].

We can compare also to the somewhat analogous situation in electronic structure theory, e.g. the Born–Oppenheimer potential of a single HF molecule: In a Hartree(–Fock) treatment, the best self-consistent single configuration energy due to the (fast) electronic degrees of freedom is calculated parametrically for the varying (slow) internuclear coordinate. This usually

results in overestimates of the electronic dissociation energies, excessively steep potentials and hence overestimated vibrational frequencies, even in the limit of an infinitely flexible basis (e.g. the vibrational HF fundamental is predicted near 4300 cm^{-1} at the Hartree–Fock limit [148]). By inclusion of additional electronic configurations (e.g. via configuration interaction, CI [149,150] or coupled cluster methods [151]), the internuclear potential function ultimately converges to the 'true' (still non-relativistic) Born–Oppenheimer potential and vibrational frequencies are in much better agreement with experiment (HF fundamental at 3961.42 cm^{-1}). Any resonant vibronic couplings are of course not treated by this approach (but rather irrelevant for the HF stretching fundamental). In the field of (slow) vibrations, adiabatic channels (obtained by DQMC) compare to minimum energy paths in a similar way as full CI compares to Hartree–Fock in electronic structure theory of a diatomic molecule. While specific, non-adiabatic resonances are not accounted for, off-resonant adiabatic coupling to the fast degrees of freedom is fully described. Evidence presented in Ref. [61] for $(HF)_2$ and in Section 4 for the trimer suggests that the off-resonant effects are systematic and large in hydrogen-bonded systems (particularly for light hydrogen bonded donor molecules, which give rise to high frequency hydrogen bond libration), while resonant interactions are generally small, becoming important only occasionally. A similar situation arises in the acetylenic CH-chromophore whereas for the three-dimensional stretch-bend potential of isolated aliphatic C–H chromophores [152], one finds a situation with strong 'nonadiabatic' Fermi-resonance interaction in addition to the off-resonant effects from the other degrees of freedom.

For quantum states with non-vanishing rotational angular momentum, the local quantum rigid rotor energy for a given set of rotational quantum numbers can be added to the electronic potential at each coordinate. A DQMC calculation carried out on such an effective rotational surface will contain the centrifugal effects resulting from the coupling of zero point vibrational motion and rotation. The result is exact for diatomics and provides a good description for polyatomics in the absence of *specific* Coriolis coupling. Such specific couplings are usually small for the lowest state of a given J rotational quantum number. For high J, an efficient coding of this method requires approximation formulae, since rigid asymmetric rotor diagonalization would otherwise dominate the computational effort. The case of a pseudo-diatomic, nearly prolate top ($(HF)_2$) has been dealt with in Ref. [61], where the method has been described for the first time. Here, we want to discuss the oblate top limit relevant for $(HF)_3$ and larger oligomers. The approximation formulae have to cover a substantial range of asymmetry parameters in this case, as near-prolate (open chain) configurations are quite low in energy [102,107]. We use an expression due to Mecke [153,154] for the average term value $F(J)$ of the two lowest levels ($K = J$, negligible splitting) for given J in the oblate top limit:

$$F(J) = CJ^2 + \tfrac{1}{2}(A + B)J - \tfrac{1}{8}(A - B)J\frac{2J-1}{J-1}b^*\left(1 + \left[\frac{b^*}{2}\right]^2\right) \quad (25)$$

with

$$b^* = \frac{B - A}{2[C - \tfrac{1}{2}(A + B)]}. \quad (26)$$

We have tested this approximation extensively using exact diagonalization with the program Wang [155] for a J range of 30–250 and A, B, C, b^* ranges covered by the wave functions of $(HF)_n$, $n = 3, 4, 5, 6$. The error of the approximation is found to be significantly smaller than the statistical DQMC error in all cases, whereas neglect of the third term in Eq. (25) leads to unacceptable errors. In order to obtain a vibrationally averaged (spectroscopic) C_0 rotational constant from these term values, the rotational contribution to the ground state energy $F(J)$ from DQMC calculations is normalized by $J(J + 2)$ and plotted vs. J^2. The resulting functions do not deviate significantly from linearity and the intercept ($J = 0$) immediately gives C_{eff}, an estimate for the spectroscopic C_0 constant in the absence of Coriolis contributions [156]. To rationalize this procedure, we rewrite the standard [154] centrifugal oblate top term formula for $K = J$

$$F(J) = BJ^2 + BJ + (C - B)J^2 - D_J J^2(J + 1)^2 - D_{JK}J(J + 1)J^2 - D_K J^4 \quad (27)$$

using $CJ + B \approx C(J + 2)$, $C \gg D_J$ and $J \gg 1$ to obtain

$$\frac{F(J)}{J(J+2)} \approx C - (D_J + D_{JK} + D_K)J^2 \tag{28}$$

In order to obtain an independent estimate for B rotational constants and hence for the magnitude of inertial defects [157], we use Mecke's expression [153,154] for the average of all rigid rotor levels with a given J:

$$\frac{\sum_\tau F(J_\tau)}{2J+1} = \tfrac{1}{3}(A + B + C)J(J+1) \tag{29}$$

as a rotational potential. While rovibrational interactions will usually invalidate this relationship for high J, the extrapolation to $J = 0$ provides an accurate average rotational constant $(1/3)(A + B + C)$.

The latter application exploits a general theorem (Helmann-Feynman) which can be easily derived using perturbation theory [158]:

Let $\hat{H}_0$ and $\hat{H}$ be time-independent Hamilton operators with

$$\hat{H}_\lambda = \hat{H}_0 + \lambda\hat{H}_1 \tag{30}$$

$$\hat{H}_\lambda \Psi_\lambda = E_\lambda \Psi_\lambda \tag{31}$$

$$\hat{H}_0 \Psi_0 = E_0 \Psi_0, \tag{32}$$

where Ψ_0, Ψ_λ are the lowest (real) eigenfunctions. Then, one has for $\langle\Psi_0|\Psi_0\rangle = \langle\Psi_\lambda|\Psi_\lambda\rangle = 1$ and $\Psi_\lambda - \Psi_0 = \lambda\Psi_1 + \lambda^2\Psi_2 + \cdots$

$$\frac{E_\lambda - E_0}{\lambda} = \langle\Psi_0|\hat{H}_1|\Psi_0\rangle + \lambda(\langle\Psi_1|\hat{H}_0 - E_0|\Psi_1\rangle + 2\langle\Psi_1|\hat{H}_1|\Psi_0\rangle) + O(\lambda^2) \tag{33}$$

and the $\lambda = 0$ intercept is

$$\lim_{\lambda\to 0}\left(\frac{E_\lambda - E_0}{\lambda}\right) = \langle\Psi_0|\hat{H}_1|\Psi_0\rangle \tag{34}$$

In the present case, $\lambda = J(J + 1)$ and $\hat{H}_1 = (\hat{A} + \hat{B} + \hat{C})/3$. Coriolis contributions would lead to differences between expectation values evaluated in this way and spectroscopically defined rotational constants [156], but for the systems investigated here, anharmonic effects are expected to dominate. Other useful applications include $\lambda = |\vec{\mathscr{E}}|/|\vec{e}|$, $\hat{H}_1 = \vec{\mu}\vec{e}$, where $\vec{e}$ is the unit vector of a homogeneous electric field $\vec{\mathscr{E}}$, and $\lambda = |\vec{\mathscr{E}}|^2/|\vec{e}|^2$, $\hat{H}_1 = \vec{e}\underline{\alpha}\vec{e}$, where $\underline{\alpha}$ is the polarizability tensor. In the latter cases, care has to be exercised to achieve a correct orientation of the molecule in the laboratory frame, as the quantities to be determined are vectors and tensors. For moderate amplitudes, the Eckart conditions [159] provide an appropriate reference frame [125]. It should be noted that it is significantly more economic to use positive and negative values for λ, as this replaces the critical extrapolation by an interpolation in the linear regime of the perturbation. The method introduced in Ref. [158] has also been applied to kinetic energy contributions and quadrupole coupling constants [160] and an improved variant of the technique has recently been published [161].

Details of the employed DQMC algorithms such as the exact monomer importance sampling strategy and choices for parameters are described in Ref. [61]. Sampling correlation corrections were carried out according to the procedure described in Ref. [162] and were found to be consistent with those obtained in simpler analyses [61].

A side result of DQMC ground state calculations is the sampling of multidimensional configuration space. As discussed earlier in this section, this can be exploited for the generation of ab initio data. For larger oligomers, it also provides a crucial first step for finding global minima [163]. The discrete wave function distribution at the end of a long and well-equilibrated DQMC run samples the potential regions relevant for the ground state. This normally includes the region around the global potential minimum, unless zero point energy effects favour a higher, but more extended valley. In any case, the wave function will sample the *physically relevant* region for very cold clusters. By using this discrete wave function distribution as an ensemble of start structures for Metropolis Monte Carlo and other conventional minimizers [164], the global minimum is located with high likelihood. Unfavourable start configurations can penetrate barriers very efficiently via quantum tunneling and thus find their way to the global minimum. Similar to temperature in simulated annealing, the particle masses (or $\hbar$) can be scaled to assist equilibration. The technique is related to other quantum methods proposed recently (Refs. [165,166] and in particular the efficient deterministic

scheme proposed in Ref. [167]), but the historically earlier DQMC realization appears to be the variant which is most easily applicable to high dimensional, highly *coupled* situations, as it profits from the simplicity and generality of the transport equation isomorphism in cartesian space (see also the recent description in Ref. [168]).

From a conceptual standpoint, DQMC-preconditioning of conventional minimizers, as we propose and use it, automatically points at the limits of asking questions about global minima. As experimental data always include zero point energy, it is quite pointless to locate minima for cases where the ground state wave function is delocalized over a wide range of structures.

3.5. DQMC using Voronoi step representation

The multidimensional DQMC sampling idea discussed above can be carried one step further. As described in detail in Refs. [82,83], one can avoid the use of an analytical Born–Oppenheimer potential and rather use some sort of multidimensional interpolation between discrete potential energy points (VQMC-DPR [82]). This removes the labour and bias of global analytical fitting but requires a robust multidimensional interpolation method.

Interpolation in truly multidimensional space is a difficult problem, but we have found [82] that representation of the potential in steps defined by Voronoi polyhedra [169,170] around the sample points works impressively well and we have thus applied this technique in the present work. The concept is based on finding the nearest neighbour reference configuration for which the potential energy is known. At the desired molecular configuration, this nearest neighbour energy is simply adopted, probably the crudest variant of interpolation. The influence range of a selected reference configuration in a multidimensional ensemble of such configurations is circumscribed by a convex polyhedron, whose definition goes back to Voronoi [169]. It remains to define an appropriate metric in the multidimensional space of internal degrees of freedom. While this is a largely unexplored field, we currently use inverse interatomic distances (squared for computational convenience), as these have the global property of being sensitive where the potential is steep. Summing over the squared differences of all (independent) reciprocal interatomic distances yields a measure for the degree of nearness between two molecular configurations. The three-body potential can be expressed as a function of the three FF distances, the three HH distances and the nine HF separations. This is a redundant set of coordinates, but it guarantees an unambiguous construction of the geometry, whereas the FF and HF distances alone do not distinguish between certain out-of-plane conformers. Permutation symmetry for the HF units is explored in the neighbourhood evaluation, as is monomer integrity [82].

Here, we use the *existing* 1004 ab initio three-body points in a Voronoi step interpolation as a start to dynamically generate and accumulate more important three-body configurations [82,83], whereas the pair potential is implemented analytically.

3.6. A more global three-body potential (HF3BG)

The analytical HF3BL potential is of limited use for larger HF clusters, as sampling and weighting for the fit concentrate on the trimer species. We have thus exploited the Voronoi representation concept described above to obtain a more global three-body point sample and fit. For this purpose, we have dynamically added new DZP + MP2 − BSSE points from several quantum and mixed quantum-classical Monte Carlo simulations of $(HF)_n$ ($n = 3$–8) at temperatures between 0 and 473 K up to a total of 3000 point samples in 12 dimensions with 3-body energies ranging from −76 to +23 kJ/mol, using different energy and distance criteria for accepting new configurations. The mixed quantum-classical simulation is decribed briefly in Ref. [83]. It is used to sample more of the heavy-frame amplitude than a quantum ground state simulation. In these simulations, an analytical pair potential is combined with a permanently updated step-interpolated three-body potential, which always comprises all currently available ab initio data. In each of the simulations, saturation of the accessible configuration space was observed, the need for new points slowing down systematically. The enlarged data base was subsequently used in a global, unweighted analytical fit (HF3BG, see [1]), similar to the HF3BL [102] one, but more flexible and involving only atomic centers (i.e. using F–F distances instead of center of mass distances in the potential expression

and fit). In the notation of the HF3BL potential, the HF3BG potential consists of the leading 3-body induction term $V_{\rm ind}^{\rm 3B}$ (the interaction centers now coinciding with the F atoms; we retain the factor 1.11 in the dipole moment function, Eq. (14), thus increasing the dipole moments somewhat, but one might also choose 1.06 to reproduce the HF3BL dipole) and a sum of exponentials V_E:

$$V_{\rm E}/(6\times 10^5\ {\rm cm}^{-1}) = \sum_{j=1}^{n}\sum_{k>j}^{n}\sum_{l>k}^{n}(8T_1 + 2T_2 - 3T_3 + 60T_4 + 90T_5 - 2T_6 - 9T_7) \tag{35}$$

with

$$T_1 = {\rm e}^{-(3/8a_0)(r_{ij}+r_{jk}+r_{ki}+r_{ik}+r_{kj}+r_{ji})} \tag{36}$$

$$T_2 = {\rm e}^{-(3/4a_0)(r_{ik}+r_{jk}+t_{ij})} + {\rm e}^{-(3/4a_0)(r_{ij}+r_{kj}+t_{ik})} + {\rm e}^{-(3/4a_0)(r_{ji}+r_{ki}+t_{jk})} \tag{37}$$

$$T_3 = {\rm e}^{-(3/4a_0)(r_{ij}+r_{jk}+r_{ki})} + {\rm e}^{-(3/4a_0)(r_{ik}+r_{kj}+r_{ji})} \tag{38}$$

$$T_4 = {\rm e}^{-(3/2a_0)(r_{ij}+r_{jk}+r_{ii})} + {\rm e}^{-(3/2a_0)(r_{ik}+r_{kj}+r_{ii})} + {\rm e}^{-(3/2a_0)(r_{ji}+r_{ik}+r_{jj})} + {\rm e}^{-(3/2a_0)(r_{jk}+r_{ki}+r_{jj})} + {\rm e}^{-(3/2a_0)(r_{kj}+r_{ji}+r_{kk})} + {\rm e}^{-(3/2a_0)(r_{ki}+r_{ij}+r_{kk})} \tag{39}$$

$$T_5 = {\rm e}^{-(3/2a_0)(r_{ik}+r_{ji}+r_{ii})} + {\rm e}^{-(3/2a_0)(r_{ij}+r_{ki}+r_{ii})} + e^{-(3/2a_0)(r_{jk}+r_{ij}+r_{jj})} + {\rm e}^{-(3/2a_0)(r_{ji}+r_{kj}+r_{jj})} + {\rm e}^{-(3/2a_0)(r_{ki}+r_{jk}+r_{kk})} + {\rm e}^{-(3/2a_0)(r_{kj}+r_{ik}+r_{kk})} \tag{40}$$

$$T_6 = {\rm e}^{-(0.88/a_0)(t_{ij}+t_{jk}+t_{ki})} \tag{41}$$

$$T_7 = {\rm e}^{-(1.38/a_0)(r_{ij}+r_{jk})} + {\rm e}^{-(1.38/a_0)(r_{ik}+r_{kj})} + {\rm e}^{-(1.38/a_0)(r_{ji}+r_{ik})} + {\rm e}^{-(1.38/a_0)(r_{jk}+r_{ki})} + {\rm e}^{-(1.38/a_0)(r_{kj}+r_{ji})} + {\rm e}^{-(1.38/a_0)(r_{ki}+r_{ij})} \tag{42}$$

$V_{\rm ind}^{\rm 3B} + V_{\rm E}$ is damped at large negative energies (and enhanced for large positive energies, which should be constrained below $12000\ {\rm cm}^{-1}$) using a simple rational function:

$$V_{\rm HF3BG}/{\rm cm}^{-1} = \frac{-1}{\left(\frac{1}{12000} - \frac{{\rm cm}^{-1}}{V_{\rm ind}^{3B} + V_E}\right)} \tag{43}$$

This three-body potential has an unweighted rms deviation from the 3000 DZP + MP2 − BSSE points of $149.8\ {\rm cm}^{-1}$, which is acceptable for the global spread of the data points. The trimer-weighted rms deviation (weights as for the HF3BL function) is $88\ {\rm cm}^{-1}$ for the full set of 3000 points and only $56\ {\rm cm}^{-1}$ for the initial set of 1004 points. This shows that the global HF3BG potential is competitive with the more local HF3BL expression for trimer simulations. The limits of the more local HF3BL potential are reflected in large rms deviations of $261.7\ {\rm cm}^{-1}$ (weighted) and $433.8\ {\rm cm}^{-1}$ (unweighted), when the data base is extended from the 1004 points employed in the HF3BL fit to the global 3000 point set.

We thus have two analytical potentials of similar quality for the trimer dynamics and a clearly superior HF3BG potential for the dynamics of larger oligomers.

4. Results for $(HF)_3$ and its isotopomers

4.1. Minimum properties

An immediate test for the analytical HF3B(L,G) potentials in conjunction with the available accurate HF pair potentials is the comparison of the C_{3h} minimum geometry and well depth of $(HF)_3$ with results from the pure and effective pair potentials. This is shown in Table 4, which may also be compared to the DZP + MP2 results in Table 2. Some key results have been summarized in Table 2 of Ref. [26] and in Refs. [102,105,119], where detailed comparison to earlier ab initio values and discussion of the BSSE issue can also be found. We use three different HF pair potentials for the trimer results. The SQSBDE potential is well documented [61] and has been shown to give a good representation of the intermolecular interaction in $(HF)_2$. Based on 6-D calculations with adiabatically separated HF stretching modes [62,106], two related variants SNB and SNC have been developed [26]. They differ from

Table 4
$(HF)_n$ ($n = 3$–6) minimum geometries, well depths (D_e/kJ mol^{-1}) and binding energies (harmonic estimates D_0^h, and fully anharmonic results D_0, in kJ mol^{-1}) for dissociation into monomers predicted by the analytical HF3B(L,G) terms (added to the empirically refined ab initio pair potentials SQSBDE [61], SNC [26,62,106], SC-2.9 [63]). Coordinate definitions are taken from Table 1. For $n = 3$, some benchmark ab initio calculations are also given. For further comparison to ab initio results, see Ref. [26,81,102]. HF2-X is an effective pair potential from the simulation of liquids [93] extended to flexible monomers [91] (see also Ref. [105])

n	r_{HF} (pm)	R_{FF} (pm)	∠FFH (deg)	D_e	D_0^h	D_0	Source
3	93.3	257	22.6	64.3	41.8	43.6	HF3BG + SC-2.9 pair potential
	92.6	271	24.4	53.2	34.5		SC-2.9 pair potential only
	92.9	258	24.4	60.7	41.8	43.3	HF3BL + SNC pair potential
	92.3	273	26.5	50.9	34.3	36.0	SNC pair potential only
	93.2	257	24.4	60.8	42.2	42.8	HF3BL + SQSBDE pair potential
	93.3	255	24.3	61.3	42.0	42.6	HF3BG + SQSBDE pair potential
	92.9	276	20.2	71.0			HF2-X pair potential [91]
	93.3	259	21.4	67.2	45.5		[5s4p2d/3s2p1d] + MP2 (this work)
				57	39		[5s4p2d/3s2p1d] + MP2 − (BSSE + MR)
	93.4	262	21.6	60.9			[8s6p2d/6s3p] + MP2 (this work)
				55			[8s6p2d/6s3p] + MP2 − (BSSE + MR)
4	94.0	251	11.6	111.6	79.0	80.6	HF3BG + SC-2.9 pair potential
	93.2	254	13.4	104.8	77.7	79.3	HF3BL + SNC pair potential
	92.4	268	14.2	87.0	61.3	63.6	SNC pair potential only
	94.4	243	12.4	113.6	82.5	83.0	HF3BG + SQSBDE pair potential
5	94.0	251	6.4	147	107	108	HF3BG + SC-2.9 pair potential
	93.0	256	7.1	134	101	102	HF3BL + SNC pair potential
	Non-planer			113		84	SNC pair potential only
	94.5	241	7.1	153	112	113	HF3BG + SQSBDE pair potential
6	93.9	252	3.3	180	131	132	HF3BG + SC-2.9 pair potential (C_{6h})
	93.0	260	3.3	157		118	HF3BL + SQSBDE pair potential (C_{6h})
	94.3	242	3.6	186	138	138	HF3BG + SQSBDE pair potential (C_{6h})

each other by a direct HF–HF stretch coupling term (S = semiempirical, N = new form, B = best, C = with additional coupling) but are otherwise quite similar. Finally, two very recent, much improved pair potentials SC-2.9 and SO-3 [63] are used in some cases.

From Table 4, it can be seen that the three-body term has a marked influence on the equilibrium FF distance and on the well depth. The hydrogen bond is contracted by 10% and strengthened by 20% upon inclusion of the three-body contributions. Variations in the pair potential are less pronounced, whereas BSSE corrections are very significant. This becomes particularly evident in Table 2, where minimizations

on the BSSE-corrected surface are also shown for comparison.

4.2. Zero point energy and predissociation

The experimentally observable binding energy D_0 can be calculated from the well depth D_e by subtracting the difference in zero point energies between the trimer and three isolated monomer fragments. This subtraction is usually carried out at the harmonic level, which is the only one easily accessible to conventional ab initio calculations. The resulting harmonic binding energies D_0^h for the combined (1 + 2 + 3)-body potentials fall within the range covered by ab initio calculations with and without BSSE correction [27,105,119], as illustrated in Table 4.

With the help of DQMC, fully *anharmonic* binding energies D_0 are available for the analytical potentials. They are also shown in Table 4. The *relative* size of the anharmonicity correction to the trimer binding energy D_0 is considerably smaller than for $(HF)_2$ [61] (3–5% in $(HF)_3$ vs. 6–8% in $(HF)_2$). This is mainly due to the more strongly bound character of $(HF)_3$ and may also have some contribution from partial cancellation of positive and negative effects. As we will see below, even this comparatively small anharmonicity effect in the ground state of $(HF)_3$ and its isotopomers has a qualitative influence on the predicted vibrational dynamics. Furthermore, as in the dimer [61], anharmonicity contributions to vibrational transitions can be much larger [110,121] (see also Section 4.3).

Apart from determining the stability of the trimer and dominating the thermal oligomerization equilibrium $HF + (HF)_2 \rightleftharpoons (HF)_3$ the precise value of D_0 is important for the discussion of possible predissociation mechanisms of $(HF)_3$ upon HF stretch excitation. In this context, the doubly degenerate IR-active HF stretch fundamental ν_5 near 3712 cm^{-1} deserves a closer examination, since it has been investigated experimentally in some detail [171]. There are two types of dissociation channels available to $(HF)_3^*$ excited by one quantum of ν_5:

$$(HF)_3^* \rightarrow (HF)_2 + HF \qquad \text{(type I)} \qquad (44)$$

$$(HF)_3^* \rightarrow 3HF \qquad \text{(type II)} \qquad (45)$$

where the type II process can also proceed in a sequential manner:

$$(HF)_3^* \rightarrow (HF)_2^* + HF \rightarrow 3HF \qquad \text{(type IIa)} \qquad (46)$$

The type I channel involves cleavage of *two* hydrogen bonds, whereas in the type II process, *three* bonds are ultimately broken. In both cases, *single* hydrogen bond cleavage via IVR induced ring opening [107,108]

$$\text{cyclo-}(HF)_3^* \rightarrow (HF - HF - HF)^* \qquad (47)$$

may be a first [38,171], and possibly the rate determining [18] step for predissociation. The lowest type I channel has an excess energy of 1060–1260 cm^{-1} (as obtained from the $D_0\{(HF)_3\}$ data in Table 4 and $D_0\{(HF)_2\}/hc = 1062\ cm^{-1}$ [11,172]) which has to be distributed among the fragments. For the lowest channel of type II, this excess energy is predicted to be only 0–200 cm^{-1}. Here, the uncertainty is dominated by ab initio and fitting errors in the combined pair and three-body potential energy functions, whereas the statistical dynamical error of the quantum simulation is negligible ($<10\ cm^{-1}$). We can thus assume that $(HF)_3 \rightarrow 3HF$ dissociation channels are open for the $(HF)_3$ ν_5 state, at least with a small amount of thermal rotational excitation available in the cluster. Previous work suffered from large uncertainties both in D_e as well as in the anharmonicity contribution to D_0. On the other hand, it is now clear that this type II dissociation, where available, must be very close to resonance. Less than three rotational quanta in the HF fragments are needed to absorb virtually all the excess energy. Depending on whether the process occurs via direct coupling to the continuum or sequentially via ring-opening and/or an excited dimer, this could lead to strongly state dependent linewidths in the ν_5 band. Experimental evidence supports the off-resonant channel I as the main pathway to dissociation [171], thus masking possible non-statistical effects from type II channels. The dominating channel I propensity can have several reasons:

(i) Given the current uncertainty in the binding energy, we cannot exclude that most type II channels for the ν_5 rovibrational states populated in the excited jet in Ref. [171] are closed.
(ii) If predissociation proceeds sequentially, it is

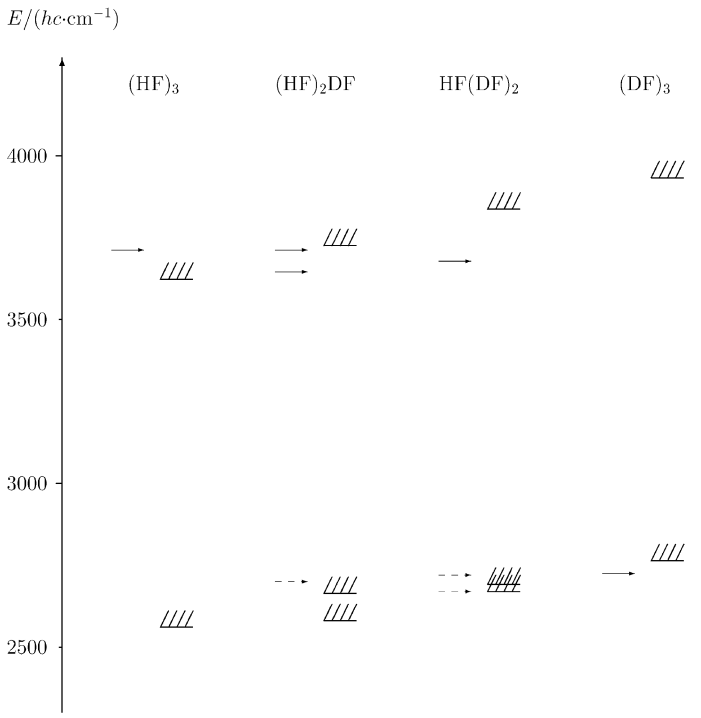

Fig. 3. Available $([H,D]F)_3$ predissociation channels (horizontal bars with symbolic indication of the fragment continuum, on the right hand side of the isotopomer double columns) upon IR-active HF- and DF-stretch excitation (horizontal arrows on the left hand side of the double columns [107,171]). The dashed arrows refer to predictions for IR-excitations which have not yet been investigated or whose assignment remains ambiguous [171]. The absolute error for the minimal channel energies (horizontal bars) is estimated to be less than 100 cm^{-1}, whereas the relative error can be expected to be much smaller. Experimental confirmation of one critical channel thus leads to very much improved estimates for all isotopomeric trimer binding energies.

possible that many excited dimer fragments do not carry enough internal energy to dissociate, whereas a direct type II process can be considered as improbable, because the reverse three body process is considered as improbable as well.

(iii) Type II predissociation as a direct (impulsive [172]) process may be intrinsically unfavourable due to the *three* diatom fragments involved, although simple energy-, momentum- or angular momentum gap laws [173] tend to favour a closely resonant channel.

(iv) From a statistical standpoint, the number of available product channels with low translational energy is vastly larger for type I processes as compared to type II reactions, due to the difference in state density in the dimer and monomer units.

Independent on the variety of dynamical scenarios for ν_5 predissociation in $(HF)_3$, the energy balance considerations inferred from the analytical potential remain valid and suggest that $(HF)_3$ predissociation is very different from predissociation of $(HF)_2$ [9,18,19,172].

Successive isotopic substitution of HF molecules by DF in $(HF)_3$ allows for an interesting tuning of the nearly resonant type II dissociation channel discussed above, which is summarized in Fig. 3 (see also Table 2 in Ref. [102], with slight changes due to improved experimental and theoretical dimer dissociation energies). While the type I channel excess energies for $(HF)_3$, $(HF)_2DF$ and $HF(DF)_2$ are all in the 950–1200 cm^{-1} range and therefore far off resonance, the calculated minimal type II channel excess energies undergo a sign change in the same series. Due to residual errors in the potential energy surface, this crossover might be limited to states with non-zero

angular momentum, but we predict that it will happen within the energy spread covered by a typical supersonic jet expansion. Although the dynamical effects of this type II channel crossing may be masked by type I channel propensity, a detailed experimental investigation should be attempted, as it could give valuable insights into the predissociation dynamics and accurate information on the cluster energetics.

A more direct dynamic prediction could be made [102] for the degenerate DF-excitation of $(DF)_3$, which was subsequently detected in the gas phase at 2724.60 cm^{-1} [103,107] after an ambiguous isotopomer assignment ($(DF)_3$ or $(DF)_2HF$) via predissociation spectroscopy at 2720 cm^{-1} [171] and matrix assignments at 2717 cm^{-1} (Ar) and 2720 cm^{-1} (Ne) (3-D anharmonic prediction in the SNB + HF3BL potential: 2733 cm^{-1}, see Refs. [103,106]). In this case, type II channels are *not* accessible and we predict the lowest type I channel to be slightly *above* resonance with the vibrational level (see Fig. 3). This provides a sensitive probe for bounds of $D_0\{(DF)_3\}$, since the experimental spectrum will either show or not show dissociation lifetime broadening for single rovibrational states. The findings of the subsequent high resolution investigation [107] are consistent with $D_0/hc > 2725\ cm^{-1}$ for the type I channel in $(DF)_3$, i.e. a stable, non-predissociative ν_5 state, although they cannot rigorously exclude predissociation on a timescale longer than 3 ns. Such a slow predissociation in turn would be hard to reconcile with the observation of very fast (≈40 ps) and essentially complete IVR in this band [107], leading to the cleavage of one hydrogen bond (i.e. ring opening). Hence, it is likely that the predissociative band observed in Ref. [171] at 2720 cm^{-1} is not due to fundamental low J, K one-photon transitions in $(DF)_3$, which we expect to be invisible to a molecular beam depletion technique due to the lack of available predissociation pathways. As described in the HF-stretching case, it should be possible to tune through the dissociation channel resonance for DF stretching excitation via isotope substitution (see Fig. 3). In a sense, this leads to a very large (in principle infinite) isotope effect [174] for photoinduced DF abstraction at essentially the same excitation wavenumber. Hence, a detailed study of mixed isotopomers can lead to a very accurate spectroscopic determination of the trimer binding energy. Observation of any predissociative mixed trimer band in the 3.7 μm region would immediately yield rather tight upper and lower bounds for D_0 in combination with the findings for $(DF)_3$ [103,107]. Bolometric detection [11] would be particularly informative, as it can discriminate between predissociative and stable excitations.

In conclusion, the $([H/D]F)_3$ system contains a number of fortunate energetic coincidences in the HF/DF stretching range, which can be explored for the study of predissociation mechanisms in hydrogen bonded systems. We emphasize that these coincidences depend rather critically on an accurate description of the pair potential, on the inclusion of three-body effects and on anharmonic contributions to the zero point energy [26,27,103].

4.3. Vibrations

Another important dynamical region of $(HF)_3$ is spanned by the intermolecular vibrations below the lowest dissociation threshold of about 2600 cm^{-1}. Here, the absence of predissociation enables spectroscopic line resolution for low enough temperatures and frequencies. This has already been established impressively for certain combination bands in the CO_2 laser range [35] whose vibrational assignment is however difficult since a large number of stretch–bend and bend–bend combinations is available and off-resonant interactions between stretching and bending manifolds have been neglected in the theoretical analysis [35]. The C_{3h} symmetry [102,105,107,171] present in $(HF)_3$ leads to three infrared active low frequency fundamentals. Rather sharp $(HF)_3$ peaks assigned to these fundamentals were found in rare gas matrices [175,176] and provide very valuable constraints for band centers, but the expected matrix shifts render predictions for gas phase values uncertain. In the gas phase equilibria, $(HF)_3$ is not very abundant [104] and most of the observed broad bands [18,104,109,177,178] are most likely dominated by contributions from larger clusters.

Table 3 summarizes the harmonic frequencies obtained from the combination of our HF pair potentials [61–63,106] with the HF3BL and HF3BG three-body potentials. One can observe a substantial stiffening of the hydrogen bond librational and stretching degrees of freedom with the inclusion of

the three-body term. A further increase in the anisotropy of the hydrogen bond potential is found when switching from the SQSBDE and SNC pair potential to the more reliable SC-2.9 pair potential. This is consistent with the findings in $(HF)_2$. Agreement with direct ab initio predictions given in Table 3 is quite close for the HF3BG + SC-2.9 potential and reasonable for the purely intermolecular MMC (molecular mechanics for clusters) model [121]. A recent diatomics in ionic systems (DIIS) model performs poorly for the out-of-plane and FF stretching fundamentals of $(HF)_3$, in line with similar deficiencies for $(HF)_2$ [89].

From the results on D_0 and on $(HF)_2$ [63,179], one can speculate that the anharmonic band centers for these low frequency fundamentals will on average be lower than the harmonic results and should not deviate by more than about 30% from the harmonic numbers. Multidimensional anharmonic calculations carried out in the HF3BL + SNB potential indeed show anharmonicity effects in the −(15–20)% range [102,106] (see also Refs. [35,121] for a reduced dimensionality treatment neglecting angular–radial coupling). These calculations involve a wide range of techniques, including varaitional/DQMC 3D–9D adiabatic separations, fixed, symmetry-constrained, and variational node DQMC calculations. In some cases, they provide rigorous upper bounds, in other cases estimates of the lowest five fundamentals of the trimer and some combinations. The results underscore the importance of vibrational treatments beyond the harmonic approximation, using methods such as DQMC [61,106], close coupling and variational calculations [62,179] or approximate angular–radial and angular–angular separation schemes in some favourable cases [35,37]. The HF3B three-body potentials are an important prerequisite for such studies, and will greatly assist the prediction and analysis of the far infrared spectrum of $(HF)_3$, its isotopomers and higher oligomers [24].

In the HF stretching range, comparison to experiment is already possible. The harmonic predictions (Table 3) for the infrared active degenerate HF stretching vibration range from 3868 to 3950 cm^{-1}, depending mostly on the employed pair potential. The more reliable pair potentials predict a harmonic shift relative to the monomer of about $-250\ cm^{-1}$, in accordance with the harmonic DZP + MP2 result *and* with the anharmonic experimental value of $-249\ cm^{-1}$. Anharmonicity within the HF stretching manifold increases the harmonic shift to about $-300\ cm^{-1}$ [106,110], whereas zero point energy contributions in the hydrogen bond modes counteract this increase to a large extent [27,63,110], thus explaining the apparent success of harmonic shift predictions. This important compensating effect of the zero-point motion is still not widely appreciated. It is a straightforward result of the weakening of the hydrogen bond due to its librational zero-point energy, which reduces the softening of the monomer mode relative to the minimum structure. In the language of spectroscopic perturbation theory, it is an important coupling term involving the HF stretching mode and the hydrogen bond modes. Quite independent of these anharmonic subtleties, the three-body effect on the HF stretching frequency shift is very pronounced, roughly doubling the value obtained without three-body contribution (Table 3).

4.4. Rotation around the symmetry axis

Equilibrium rotational constants for the (H/D) isotopomers of $(HF)_3$ are summarized in Table 5 for some analytical potentials and can be compared to the ab initio results given in Tables 2 and 6 as well as in Ref. [88]. Comparison of pair potential results with those including HF3BL three-body interaction underscore the structural importance of cooperativity. The equilibrium rotational constants are not directly observable, as zero point vibrational motion couples to rotation. For rotation around the three-fold symmetry axis, we have obtained coupled C_0 constants within the framework of effective rotational surface DQMC, as described in Section 3. These are also shown in Table 5. Vibrational correction at the ground state level is relatively small due to partial cancellation of stretching and bending effects, but significant. It brings the theoretical prediction into agreement with the recent experimental [107] C_0 value for $(DF)_3$ within statistical error bars. Independent evaluation of B_0 via Mecke's sum formula [153] also confirms the negligible inertial defect in the $(DF)_3$ ground state found in the experimental spectra [107]. This *close* absolute agreement between theory and experiment must be considered somewhat fortuitous in view of the possible ab initio and fitting error in the analytical

Table 5
Rotational constants for $(HF)_3$ and its isotopomers in cm^{-1} at equilibrium (index e) and including coupling to zero point motion (index 0; from DQMC with statistical error bar; C_0 and $B_0/2$ are obtained independently using the Mecke formulae discussed in the text and show no significant inertial defect) for the SNB/SNC potentials (indistinguishable for the quoted accuracy) including (no upper index) and excluding (upper index pp) the three-body potential HF3BL. For $(DF)_3$, experimental data [107] are also given

Isotopomer	C_e	C_e^{pp}	C_0	C_0^{pp}	$B_0/2$
$(HF)_3$	0.1288		0.124(1)		
$(DF)_3$	0.1245	0.111	0.121(1)	0.107(1)	0.121(1)
Exp [107]:			0.120		0.120
	A_e	B_e	C_e		
$(HF)_3$	0.2575	0.2575	0.1288		
$(HF)_2DF$	0.2575	0.2519	0.1273		
$HF(DF)_2$	0.2547	0.2491	0.1259		
$(DF)_3$	0.2491	0.2491	0.1245		

potential as well as possible Coriolis corrections, which have been neglected. However, it provides first reliable (a posteriori) information on the *equilibrium* structure of this highly anharmonic system, which should be very close to the data set given in Table 4, namely $R_{FF} = 258$ pm, $r_{HF} = 93$ pm and $\angle FFH \approx 24°$. This represents a sizeable contraction of the hydrogen bond compared to the dimer value ($R_{FF} \approx 275$ pm), caused mainly by the three-body term. Based on these data, the microwave (MW) spectrum for mixed isotopomers can be predicted quite accurately (see Table 5). Mixed isotopomers are expected to have a zero point motion induced dipole moment in excess of 0.01 D due to the HF distance dependence of the monomer dipole, induction enhancement in the trimer and large amplitude bending motion. This should be sufficient for detection using FT-MW techniques in supersonic jets [1–3] and could improve structural information on the trimer beyond that obtained from the strongly coupled ν_5 spectrum [107].

4.5. Other stationary points and minimum energy paths

Investigation of the local environment around the trimer equilibrium structure gives useful qualitative insight into the hydrogen bond dynamics. Global results using DQMC techniques lead to quantitative spectroscopic information for low excitations and inspection of the associated wavefunctions indicates the absence of dramatic delocalization effects. A remaining task concerns the characterization of the potential surface far from equilibrium, in an energetic range accessible to HF stretching excitation. In this region, the ab initio data base for the HF3BL three-body potential is relatively sparse, whereas the extended HF3BG data base should be sufficient for a reliable description.

A first important question concerns equivalent minima. Clearly, the cyclic $(HF)_3$ hydrogen bond pattern for distinguishable HF units can be formulated clockwise (e.g. $1 \rightarrow 2 \rightarrow 3 \rightarrow 1$) and counterclockwise ($1 \leftarrow 2 \leftarrow 3 \leftarrow 1$). One may ask whether vibrational interconversion tunneling [178] between these clock- and counterclockwise hydrogen bonded cyclic $(HF)_3$ minima is feasible and whether it will be visible in the fundamental spectra. The barrier for such a process is expected to be much higher than in the dimer, since the odd number of constituents implies that no favourable all-disrotatory path exists in contrast to the dimer [178]. We have searched carefully for stationary points above the C_{3h} minimum of the $(HF)_3$ surface. Most of the initial searching efforts concentrated on the analytical potentials, since this is many orders of magnitude more economic than for reliable ab initio calculations. The resulting stationary points were then used as initial guesses for other analytical potential surfaces and [8s6p2d/6s3p] + MP2 analytical gradient calculations (Table 6). Only three additional stationary points were found and vibrationally analysed using a smaller [5s4p2d/3s2p1d] basis set at MP2-level. Energetically, they are all quite close to the type I dissociation channel products. Hence, they correspond to very floppy metastable or transition structures with sizeable zero-point energy differences already at the harmonic level, which might even be amplified by the inclusion of anharmonic effects [145]. This is in contrast to the dimer C_{2h} interconversion transition state which is quite tight, at least at the anharmonic level [145]. Due to the weak binding and relatively large monomer distances, three-body interactions are much less important than close to the minimum. In fact, the three stationary geometries can be described conveniently by two $(HF)_2$ near-minimum structures having their donor or acceptor HF molecules merged, i.e. in a

Table 6
Stationary points of HF trimer calculated at the MP2 level using the [8s6p2d/6s3p] basis set described in the text. r, R denote distances, A_e, B_e, C_e equilibrium rotational constants, D_e the total dissociation energy (into monomers). Δr_{HF} denotes the change in r_{HF} upon complexation

C_{3h}, global minimum			
D_e/hc (cm^{-1})	5090	r_{HF} (pm)	93.4
R_{FF} (pm)	262	Δr_{HF} (pm)	1.7
A_e, B_e, C_e (cm^{-1})	0.2509, 0.2509, 0.1254	∠FFH (deg)	21.6
C_s-saddle, [ad]-chain			
$E - E_{C_{3h}}/hc$ (cm^{-1})	1507	∠HF···F (deg)	116.4, 3.8, 2.3
r_{HF} (pm)	92.2, 92.9, 92.6	R_{FF} (pm)	267.8, 271.0, 468.1
C_{2v}-minimum,[aa]-structure			
$E - E_{C_{3h}}/hc$ (cm^{-1})	2743	∠HF···F (deg)	3.5 (long F···F)
r_{HF} (pm)	2 × 92.1, 92.3	R_{FF} (pm)	2 × 284.0, 547.1
C_{2v}-saddle,[dd]-structure			
$E - E_{C_{3h}}/hc$ (cm^{-1})	2869	∠HF···F (deg)	131.7 (long F···F)
r_{HF} (pm)	2 × 92.0, 92.6	R_{FF} (pm)	2 × 277.4, 323.4

pairwise additive fashion. This qualitative description immediately leads to three structures, namely a donor merged trimer ([dd]-$(HF)_3$), an acceptor-merged trimer ([aa]-$(HF)_3$) and a chain molecule obtained by merging a donor HF with an acceptor HF ([ad]-$(HF)_3$) and these are in fact the stationary geometries found by both analytical and ab initio searches (see Fig. 4).

The [dd]-$(HF)_3$ structure is a C_{2v} saddle point 2869/2682 cm^{-1} above the minimum with an imaginary harmonic frequency of about 200 cm^{-1} magnitude in the ab initio/HF3BG + SQSBDE potential. A related C_{2v} barrier of 2900 cm^{-1} has been determined using an electric dipole-type potential without radial relaxation of the equilateral $(HF)_3$ triangle [35]. From harmonic frequencies in the [5s4p2d/3s2p1d] basis, we estimate a harmonic zero-point energy correction of about −800 cm^{-1} for the threshold energy relevant in the framework of transition state theory (see however Ref. [145] for the crucial influence of anharmonicity contributions). Interconversion tunneling via this [dd]-structure is possible and profits from the small necessary displacements of the heavy nuclei along the path. However, the flatness and width of the barrier probably requires sizeable promotion by bending excitations for the spectroscopic observation of the process.

The [aa]-$(HF)_3$ structure is a local C_{2v} minimum 2743/2573 cm^{-1} (ab initio/HF3BG + SQSBDE) above the C_{3h} global minimum. The older HF3BL +

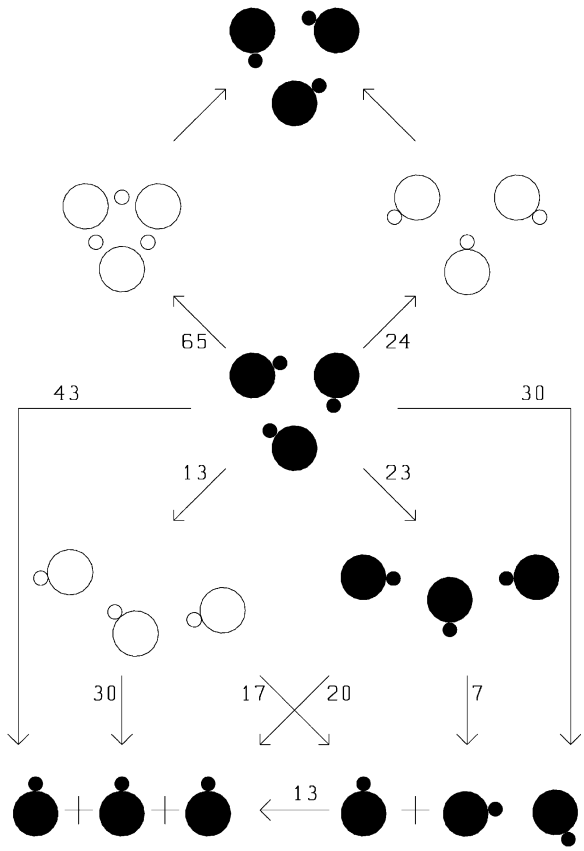

Fig. 4. Schematic representation of important rearrangements in $(HF)_3$, indicating minima (full circles) and saddle points (empty circles) together with approximate barriers and thresholds (including zero point energy) in kJ/mol.

SNB potential predicts this minimum to be considerably lower, at 2250 cm^{-1}, whereas the result for the most recent HF3BG + SO-3 potential is 2804 cm^{-1}. A somewhat related secondary minimum structure has been found for the $H_2O(HF)_2$ complex [55] and for $(HF)_3$ in a pairwise additive approach [180]. Again, the zero point energy corrected barrier is some 700–800 cm^{-1} lower, indicating a flat local environment. The barriers connecting this structure to the global clockwise and counterclockwise minima are less than about 200 cm^{-1} in the HF3BL + SNB potential, as inferred from Monte Carlo simulations. The pronounced heavy atom motion makes this path somewhat less relevant for the interconversion tunneling dynamics. Nevertheless, interconversion via the [aa] structure may be an attractive *classical* (thermal) path, since it only involves a sequence of disrotatory dimer bending motions apart from the ring opening and closure. The structure is also important for the discussion of chain *branching* in larger HF clusters and the liquid (see later sections).

Finally, the [ad]-$(HF)_3$ chain structure remains to be discussed. It has no direct relevance to interconversion tunneling, since it does not connect clock- and counterclockwise minima. However, similar to the $C_{\infty v}$ $(HF)_2$ structure, it is dynamically important, in particular for the ring opening processes discussed in the context of predissociation [38,107,171]. The lowest C_S chain structure is found to be a saddle at 1507/1579 cm^{-1} (ab initio/HF3BG + SQSBDE) with an imaginary frequency of 70 cm^{-1} magnitude. With the HF3BL + SNB potential, it is predicted considerably higher, at 1917 cm^{-1}. Zero point energy correction at the harmonic level amounts to about 400–500 cm^{-1} and thus emphasizes the dynamical importance of this structure for excited vibrational states. According to these predictions, ring opening in HF trimer should be feasible at or just beyond CO_2 laser excitation frequencies, where the cluster has already been studied spectroscopically [35]. Ring opening is definitely possible and has already been observed after monomer fundamental excitation [107].

Summarizing our findings and considering that dissociation of the trimer into a dimer and a monomer only requires about 2561 cm^{-1}, interconversion tunneling in $(HF)_3$ is a slow and complex process [181] which will be difficult to observe in the far infrared spectrum. In this sense, ground state $(HF)_3$ may be considered as less floppy than $(HF)_2$, while this does not exclude substantial anharmonicity effects. The analytical surfaces based on the HF3BG three body term appear to describe interconversion well. Ring opening to a HF–HF–HF chain conformation is energetically much more feasible than hydrogen bond interconversion. The barrier is above fundamental excitations of hydrogen bond modes and is somewhat overestimated by the HF3BL three-body potential. This suggests that anharmonic density of state estimates from this analytical potential at high energies may be somewhat too low, in good agreement with experimental estimates [107].

It is instructive to investigate minimum energy paths connecting the stationary points on the analytical surface. Fig. 5 shows such paths with respect to FFF bond angle variation. Constraining the molecule to planarity allows motion along 'excited' paths for certain ranges of the angle, as shown in the figure. The steep C_{3h} global minimum should be compared to the floppy character of higher stationary states, where deviations between HF3BL and HF3BG parameterizations are significant. Fig. 6 shows a path along a distance constraint, namely the center of mass separation R between a chosen monomer and dimer fragment. For distances up to about 450 pm, the path closely resembles the angular motion shown in Fig. 5. The distance constraint is fulfilled with angular distortions as long as possible. Only when the trimer is stretched beyond linearity, the second hydrogen bond cleavage sets in and gives rise to a steepening of the path.

4.6. Adiabatic stretching channels

As FF-stretching is a slow coordinate in $(HF)_3$, the minimum energy paths discussed in Section 4.5 are not the best reduced dimensionality potentials for this motion. Rather, the zero point energy of the remaining, faster degrees of freedom should be added [182]. This has been done for the three-dimensional FF stretching potential [106]. Here, we investigate the one-dimensional stretching potential shown in Fig. 6 as this already contains the essential adiabatic effects for the type I dissociation coordinate without being complicated by the other stretching modes. The lowest adiabatic stretching channels for relative motion of the monomer and dimer fragments

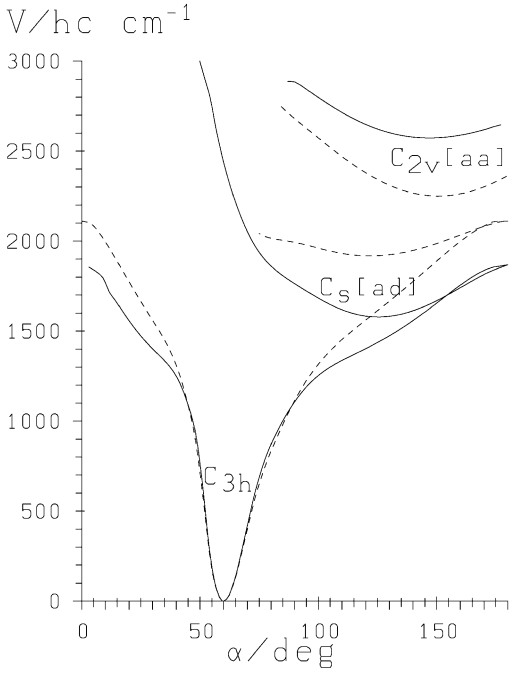

Fig. 5. Planar minimum energy paths along the $F_1F_2F_3$ angle α for the SQSBDE + HF3BG (full) and SNB + HF3BL (dashed) potentials. The lowest path goes through the global C_{3h} minimum and starts/ends at a collinear FFF conformation with off-axis hydrogens (a higher order saddle point). The two in chain hydrogen bonds are always cis-configured. If a trans-configuration such as the C_S[ad] saddle is used at the start, one can move in a secondary constrained minimum path within a certain angular range (middle curve) and the C_S[ad] saddle corresponds to a minimum on that path. Using a C_{2v} starting point leads to the highest path shown within a range of α values. This path goes through the C_{2v}[aa] stationary point. Note the agreement of the two potential functions in the hydrogen bonded region and the differences at higher energies, where the SQSBDE + HF3BG potential is based on better sampling.

have been calculated for $(DF)_3$ and $(HF)_3$ and are shown as full lines in Fig. 6. As expected, the channel for $(HF)_3$ is shallower than that for $(DF)_3$ because of the increased zero point motion for the light hydrogen isotope in the hydrogen bond modes which switch into rotations for the dissociated products. In this sense, deuterium bonds are stronger than hydrogen bonds [183,184]. There is an opposing effect due to the intramolecular frequency shift, which is larger for hydrogen than for deuterium and thus stabilizes the lighter isotopomer. This intramolecular effect, however, is smaller than the intermolecular effect in the case of HF clusters, because librational frequencies usually exceed monomer frequency shifts in magnitude. The net strengthening of the hydrogen bond upon deuteration has consequences for IR spectroscopy. While the harmonic (degenerate) prediction for the stretching fundamentals is 181 cm^{-1}/178 cm^{-1} for $(HF)_3/(DF)_3$ due to the small difference in mass, the fundamental transitions in the corresponding adiabatic channels are 153 cm^{-1}/155 cm^{-1}. This *inverse* isotope effect agrees remarkably well with experimental matrix data [176], which find 152.5 cm^{-1}/155.5 cm^{-1} for $(HF)_3/(DF)_3$. The agreement of the absolute values must be fortuitous, considering matrix shifts, ab initio errors, fitting artifacts and the reduction of the stretching problem to one dimension [61,106]. The shift, however, is a real, adiabatic off-resonant coupling effect, as discussed in Section 3. A standard minimum energy path treatment yields 174 cm^{-1}/170 cm^{-1}, i.e. wrong ordering and magnitudes. This confirms the findings in $(HF)_2$ [61] and clearly shows that hydrogen bond stretch anharmonicity is not dominated by diagonal terms but rather by the off-diagonal zero-point energy coupling or correlation. Similar effects should be found in other hydrogen bonded clusters [184], as the transformation of high frequency hydrogen bond librational modes into rotations upon dissociation is a general principle [143,144].

5. Energetics and dynamics of HF oligomers

Clusters beyond dimers are studied for many hydrogen bonded systems, but the clustering tendency of gaseous hydrogen fluoride is uniquely pronounced in terms of cluster size and concentration [18,104,106,185]. Therefore, it is worthwhile to investigate to which extent a pair + three-body potential approach will be valid for larger aggregates. Higher than three-body interactions may come into play and even if they are individually of small magnitude, their number grows quickly with increasing aggregate size n. Another limitation is given by the increasing importance of the inner two-body sampling region. While the earlier pair potentials of $(HF)_2$ have been constructed for typical dimer interactions, the nearest neighbour distance in larger clusters is considerably shortened [88,105,186] and approaches values for which ab initio sampling and spectroscopic

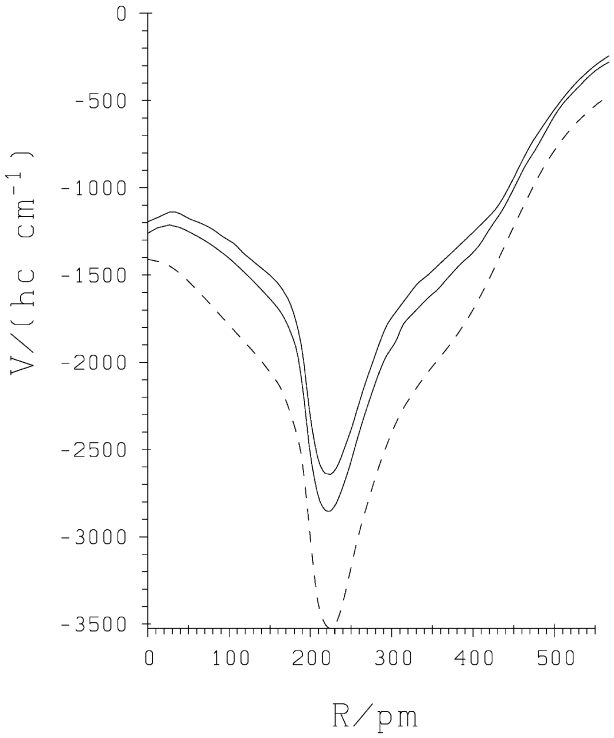

Fig. 6. 1-D minimum energy path (dashed) and $(HF)_3$ (upper), $(DF)_3$ (lower full curve) lowest adiabatic dimer–monomer stretching channels obtained from the SNB + HF3BL potential via clamped-coordinate DQMC. *R* is the distance between monomer and dimer centers of mass. All channels have been normalized to 0 for infinite separation. The sigmoid behaviour of the channels for moderate elongation marks the transition between single hydrogen bond cleavage and double hydrogen bond cleavage. A plot extending to larger distances can be found in Ref. [27], Fig. 7.

characterization of the dimer becomes sparse. This will be particularly noticeable for the HF stretching dynamics due to the extended quantum motion of the light hydrogens, while the intermolecular vibrations should initially be less affected. Thanks to the modular character of the many body approach, this can be remedied by the refinement of the HF pair and three-body potentials and eventually by the inclusion of a four-body term [26]. However, hydrogen exchange between monomer units, which is neglected in current analytical models, becomes more and more important for larger clusters [26,27,105,119]. This means that refinements beyond a certain level may require a reformulation of the potential expressions [26,187]. Here, we want to explore structural and dynamical properties of the *available* combination of pair- and three-body potentials for the next higher oligomers ($n = 4$–7) in some detail, in order to get some insight into the possible limitations mentioned above. Using the new tool of Voronoi step representation in vibrational QMC [82], one can also assess the analytical fitting bias inherent in the potentials [83].

5.1. Higher than three-body forces

A crucial test for the applicability of our approach to the simulation of larger HF clusters ($n > 3$) is provided by the ab initio evaluation of higher-body contributions in representative (close to minimum) $(HF)_n$ configurations. We have used the ab initio approach described in Section 3, i.e. the DZP + MP2 − BSSE level, to calculate all nonvanishing *m*-body contributions for a C_{5h} pentamer geometry close to the (presumably absolute) minimum found by us (FF-distance: $4.86a_0$, monomer HF-distance: $1.756a_0$, FFH-angle 7.3°) and for a C_{6h} hexamer geometry close to the optimized structure given in Ref. [88] (FF-distance: $4.677a_0$, monomer HF-distance: $1.791a_0$,

FFH-angle 0°). For the pentamer geometry, all terms turn out to be attractive. The three-body energy amounts to 42% of the two-body potential, and the succeeding terms converge exponentially (4% four-body contribution, 0.3% five-body contribution). A recent, much more accurate calculation [119] yields 64, 9, and 0.7%, respectively, at a similar geometry. For the hexamer geometry, the three-, four-, five-, and six-body contributions amount to 83, 18, −6, 2% of the two-body potential.

These numbers suggest that combined one-, two- and three-body potentials should give a reliable description of the hydrogen bond dynamics of HF clusters close to equilibrium up to at least six monomers [102], provided the analytical fits are accurate enough. The error introduced by this truncation is relatively systematic, leading to a somewhat underestimated hydrogen bond strength in larger clusters. This is also confirmed by density functional calculations [26,105] (see in particular Figs. 2 and 10 in Ref. [26]). More serious deficiencies arise for large HF bond elongations, close to concerted hydrogen transfer structures [26] and for higher order properties sensitive to derivatives of the potential energy. For clusters beyond the hexamer, non-bonded contacts start to come into play and may be more sensitive to subtle many-body contributions. For solid and liquid HF, at least a substantial improvement over $(HF)_2$-derived pair potentials is expected.

5.2. Oligomer structure and stability trends

Given the predicted usefulness of a combined (1 + 2 + 3)-body approach for larger HF clusters, we have to explore the reliability of the *analytical fits* involved. For this purpose Tables 3 and 4 contain results for higher oligomers. The minimum geometries for the analytical surfaces have been obtained by various techniques, ranging from Metropolis Monte Carlo techniques with simulated annealing to methods involving the calculation of the Hessian matrix [188]. Due to the rapidly increasing number of local minima, there is no strict proof that the lowest minima found are in fact the global ones. However, many independent runs render this very likely for $n \leq 6$. Harmonic analysis of the structures was always used to confirm that they correspond to a minimum.

The global minima for clusters of 3–7 HF units are simple rings with each HF engaging in one hydrogen bond as a donor molecule and in one as an acceptor [26,27,88,102,105,109,119]. A general *qualitative* question about these ring structures concerns their planarity. While the quantum nature of nuclear motion may wash out the transition between planar and non-planar structures to some degree, the equilibrium structure is defined in a classical sense as a property of the electronic potential energy surface. True and effective pair potentials tend to predict folded rings already for $n = 4$ (HF2-X [91]) or $n = 5$ (SNB/C [26,27]), while inclusion of three body forces leads to planar (C_{nh}) global minima for all oligomers up to and including the pentamer. For $n = 6$, we find a transitory behaviour with competitive planar and folded structures, while larger clusters are clearly folded. This might be related to the regular pentagon being the largest equilateral, isogonal polygon constrained to lie in a plane [189], but more likely it is due to the existence of residual ring strain up to this size. The ab initio DZP + MP2 calculations shown in Table 2 locate the transition to non-planarity between $n = 5$ and $n = 6$ and predict the planar C_{6h} structure of $(HF)_6$ to be a third-order saddle point, whereas the geometry at the global minimum is a S_6 chair conformation 0.7 kJ/mol lower in energy. If confirmed, this would be a particularly simple example for the rare S_6 point group, which requires at least 12 atoms to be realized. In between these conformations, boat-like and twist-like stationary points of C_2 symmetry can also be found (Table 2). $(HF)_6$ is thus very close to the quasiplanar [157] limit. This is even more pronounced when zero point energy is added to the three-dimensional puckering potential around the 3rd order C_{6h} saddle, not counting any contributions from the three low frequency puckering modes. Such an adiabatic potential of puckering motion in the bath of faster bending and stretching modes is expected to be closer to the reality than the simple electronic puckering potential where the remaining degrees of freedom are minimized [61,143]. In this adiabatic potential, we find at the DZP + MP2 *harmonic* frequency level that the C_{6h}–S_6 energy difference is reduced from 0.7 kJ/mol to 0.25 kJ/mol. Inclusion of anharmonicity can be expected to lead to effects of similar magnitude [145]. Density and hybrid functional calculations

predict a very slightly non-planar S_6 structure for the hexamer [105].

Although the analytical potentials presented in this work cannot be expected to be quantitatively reliable at this level of subtle effects, it is interesting to compare their properties to the less biased (but at least for $n < 4$ much less accurate) DZP + MP2 predictions. The analytical SQSBDE + HF3B and SC-2.9 + HF3BG potentials have a global C_{6h} minimum, whereas the SNB/C + HF3BL potentials exhibit a C_{6h} *secondary* minimum, which is 0.7 kJ/mol above a presumably global, strongly folded C_2 twist-like, chiral minimum structure. When zero point energy is included at the harmonic level, the energy difference between the two minimum structures reduces to only 0.1 kJ/mol. A large number of further low energy minima and extended flat valleys can be found in this potential surface and examination of the ground state wavefunction generated by DQMC indicates that it has significant amplitude in several of these minima and valleys. The barriers separating the stationary points (minima) are low and therefore quantum delocalization is expected, although some localization is suggested by perturbation theory in the large barrier limit for non-equivalent minima.

An interesting spectroscopic consequence of the pronounced quasiplanarity of $(HF)_6$ in the SNB + HF3BL potential is found for the C rotational constant, which corresponds to spinning motion around the ring axis. The C constant differs by more than 50% for the C_{6h} structure and the structure of the global minimum of the SNB + HF3BL surface and still by about 6% for the corresponding stationary points in the DZP + MP2 approach. The *effective* zero-point averaged C_0 rotational constant, which can be obtained from DQMC calculations for high J values, appears to be quite normal, as in smaller clusters. However, it extrapolates smoothly to the planar (secondary) C_{6h} minimum value rather than to the global (C_2) one at $J = 0$. Upon rapid spinning rotation, centrifugal effects obviously invert the energy sequence. It is, however, quite unlikely that such a pronounced effect of quasiplanarity can be confirmed experimentally.

The C_{nh} symmetry of the planar ring structures reduces the number of independent structural parameters to three. The DZP + MP2 results quoted in Table 2 are expected to be reliable as far as *trends* in these structural parameters are concerned. The ∠FFH hydrogen bond angles are a measure for ring strain. The strain free value is $<10°$ already for pair interactions. Upon inclusion of three-body terms, the optimum angle may be somewhat smaller, $\approx$ 2–6°. In rings, realization of the optimum angle for a single hydrogen bond is influenced by the acceptor HF angle, which in turn is constrained by ring closure. This constraint vanishes for $n \approx 5, 6$. The resulting steady decrease [105] of ∠FFH from $n = 3$ to $n = 6$ is nicely matched by the analytical potentials, whereas DIIS models [89,122] currently overestimate the bending angles.

The FF distance R_{FF} drops steadily with increasing ring size, while the HF bond lengths r_{HF} increase in the same direction (see Table 2). These two trends are strongly correlated [105,190]. Both are consequences of the increased hydrogen bond strength and sensitive measures for the reliability of analytical fits, as the energy required to reverse these trends is rather small. This structural sensitivity is also illustrated by the difference between cluster minima obtained by BSSE correction before or after minimization (Table 2). Energy effects of the order of 2–3% cause structural changes of similar size. From Table 4, it is seen that the analytical potentials only show the correct bond length trends for $n \leq 5$. For $n > 5$, the trends are reversed. This may be a consequence of neglected higher-body forces or enforced monomer integrity. DIIS models perform qualitatively better in this respect. The recent experimental structure [24] of the tetramer is in good agreement with the ab initio and analytical potential predictions, considering both theoretical and spectroscopic data inversion uncertainties.

The difference between harmonically estimated local binding energies D_0^h and fully anharmonic global D_0 results continues to decrease beyond the trimer, amounting to less than 1% in $(HF)_{5,6}$ and therefore approaching the statistical error of the DQMC calculations, which is less than 0.5% of the dissociation energy in most cases. This may be explained by a cancellation of opposing effects for different degrees of freedom and by the strong binding in these clusters. However, neglect of hydrogen exchange pathways in the analytical potential energy surfaces may also contribute artificially to this effect.

The process of stepwise evaporation of HF

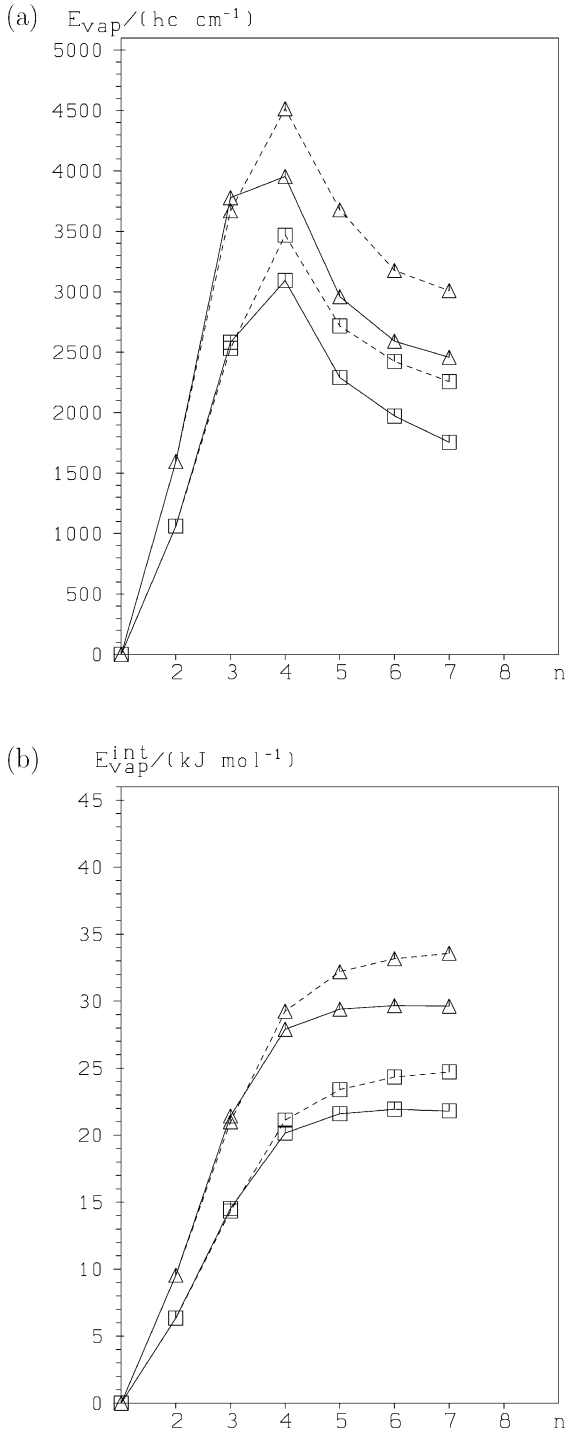

Fig. 7. (a) Stepwise vaporization energies $E_{vap}(n)$ at 0 K corresponding to the process $(HF)_n \rightarrow (HF)_{n-1} + HF$ obtained classically (△) and including anharmonic zero point energy (□) for the SC-2.9 + HF3BG potential (full lines). Also shown are the best estimates including higher than three-body forces [26] (dashed lines). (b) as in (a), but showing the integral vaporization energy per HF unit $E^{int}_{vap}(n)$ corresponding to the process $\frac{1}{n}(HF)_n \rightarrow HF$.

molecules from a cluster of size n

$$(HF)_n = (HF)_{n-1} + HF \qquad \Delta_r H^0_0 = E_{vap} \tag{48}$$

is very important in the interpretation of predissociation experiments, because it governs the open channels for cluster decay as long as cluster–cluster product channels are not favoured. The latter is certainly true for $n < 8$. Stepwise vaporization energies E_{vap} are a sensitive probe of ring strain and other hydrogen bond weakening effects, as they correspond to the energy *difference* between two neighboring clusters. For the HF3BG + SC-2.9 potential (see Table 4), they are plotted with (E_{vap}) and without (E'_{vap}) anharmonic zero point energy correction in Fig. 7a.

One can also consider the integral vaporization energies per HF unit, E^{int}_{vap} corresponding to the reaction

$$\frac{1}{n}(HF)_n = HF \qquad \Delta_r H^0_0 = E^{int}_{vap}. \tag{49}$$

These are shown in Fig. 7b. Both representations, while containing the same information, have their relative merits. The integral energies demonstrate the energetic approach to the solid and global thermodynamical stability trends, whereas the stepwise energies are directly relevant for elementary vaporization, condensation and cluster-'melting' processes.

To judge the reliability of the HF3BG + SC-2.9 potential beyond $n = 3$, Fig. 8 shows DZP + MP2 results (Table 2) for the global $(HF)_n$ minima up to $n = 8$, with and without harmonically estimated zero point energy correction. The qualitative agreement is quite good, considering the substantial BSSE inherent in the ab initio data and the lack of higher than three-body terms in the analytical potential energy surface. The latter contributions can be estimated by a detailed analysis of the ab initio calculations (Table 2) and by calculations at higher levels [26,104–106,119], also supported by spectroscopic evidence [110,111]. The

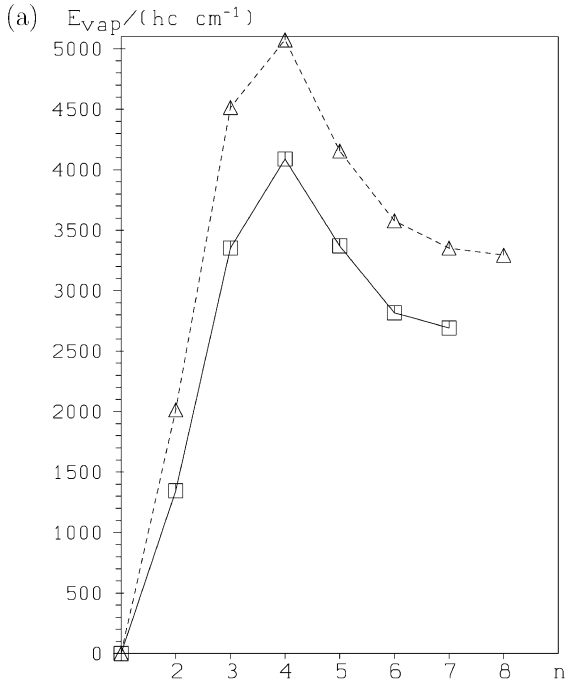

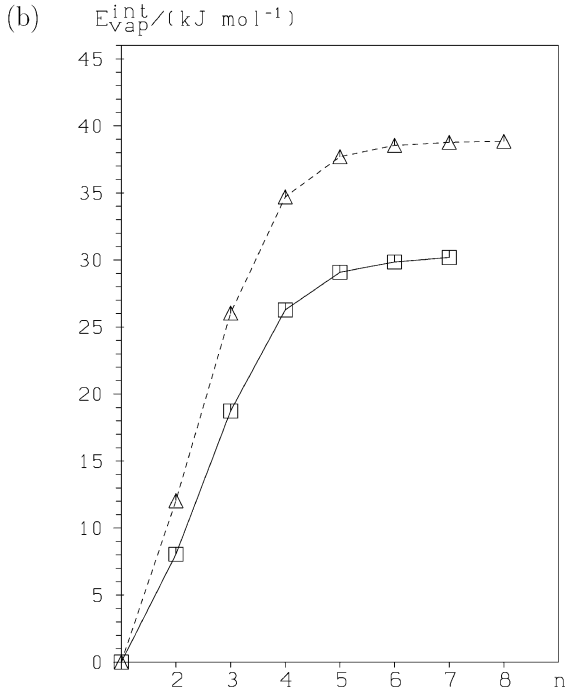

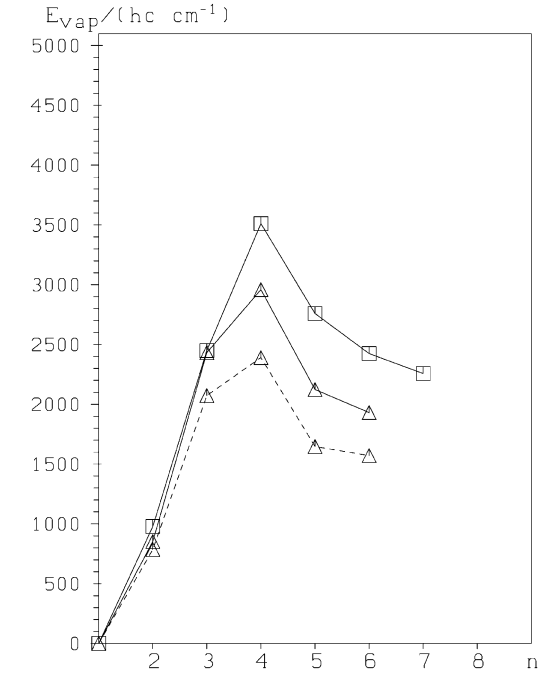

Fig. 9. Stepwise MMC [121] vaporization energies $E_{vap}(n)$ at 0 K (△) corresponding to the process $(HF)_n \rightarrow (HF)_{n-1} + HF$ including harmonic zero point energy without (dashes) and with (full line) consideration of HF stretching contributions (from our DZP + MP2 results). For comparison, best estimates for D_0^h [26] are also given (□).

current best values for the stepwise dissociation energy [26], based on such estimates, are also reproduced in Fig. 7.

A further independent assessment of the stability sequence up to $n = 6$ is provided by the intermolecular MMC (molecular mechanics for clusters) data [121], although at this level, which involves rigid monomers, the pentamer structure is non-symmetric. The data are presented in Fig. 9, which may be compared to Figs. 7 and 8. For a reliable prediction of zero point energy corrected binding energies D_0^h, it is essential to add contributions from monomer flexibility, i.e. intramolecular frequency shifts, to the rigid

Fig. 8. (a) Stepwise DZP + MP2 vaporization energies $E_{vap}(n)$ at 0 K corresponding to the process $(HF)_n \rightarrow (HF)_{n-1} + HF$ obtained classically (△, dashed) and including harmonic zero point energy (□, full line). (b) as in (a), but showing the integral vaporization energy per HF unit $E_{vap}^{int}(n)$ corresponding to the process $(1/n)(HF)_n \rightarrow HF$.

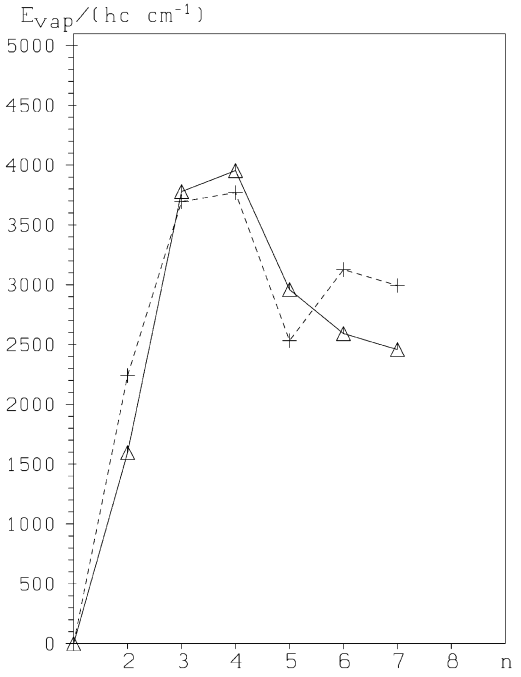

Fig. 10. Stepwise HF2-X [91] vaporization energies $E_{vap}(n)$ at 0 K (+, dashed) corresponding to the process $(HF)_n \rightarrow (HF)_{n-1} + HF$ in the classical approximation without zero point correction, compared to the HF3BG + SC-2.9 result (△). The effective pair potential substantially overestimates the dimer binding energy.

MMC data. We have done this at the DZP + MP2 level, as shown in Fig. 9. While the quantitative dimer performance of the corrected MMC results is inferior to that of the HF3BG + SO-3 potential, the qualitative behaviour for larger clusters is quite similar, indicating that an induction model with empirical repulsive components can perform quite well. However, monomer flexibility is seen to be at least as important as higher than three-body contributions for an accurate description of the larger clusters [26].

On the other hand, an *effective* pair potential such as the HF2-X model [91] may perform reasonably well on the average for larger clusters, but it will substantially overestimate the dimer binding energy, where many-body contributions are missing. This is illustrated in Fig. 10.

Comparison of the results displayed in Fig. 7 to the infinite cluster limit, i.e. the vaporization enthalpy or dissociation energy D_0^0 of the solid at 0 K, would be desirable. Due to the unusual vapor phase properties of HF [104], this quantity is quite uncertain. It can be estimated to be $D_0^0 = 34 \pm 2$ kJ/mol from a thermodynamic cycle calculation integrating the best available thermodynamic data [191–193], with the enthalpy of vaporization ΔH_{vap} into the *ideal* gas state as the most critical quantity. Despite sizeable error bars, one can see that the integral stabilities are far from convergence to the solid, whereas the stepwise vaporization enthalpy of $(HF)_4$ is likely to exceed that of the solid due to the highly strained product molecule $(HF)_3$. Turning to more qualitative aspects of cluster stability, all models predict a strong *relative* stability maximum for the tetramer, followed by the trimer and the pentamer. The dimer, whose binding energy is naturally overestimated by *effective* pair potentials, is much less stable against HF vaporization. On the larger cluster side, the pentamer, hexamer, and heptamer do not reach the relative stability level of the tetramer, as in many other systems [39,42,125,194,195]. This relative stability maximum at $n = 4$ is mainly a consequence of the strain energy in the $n = 3$ dissociation product, which is caused by the pair potential and reinforced by three body attraction [26,27,104]. In HF clusters, the strain effect is not masked by steric hindrance. In alcohol clusters, steric interactions can be systematically varied to oppose the strain effect, leading to a stabilization of smaller aggregates [196].

5.3. Oligomer isomerism

So far, only the global minimum (simple ring) structures for $(HF)_n$ with $n < 8$ including some ring puckering have been discussed. As expected for a multidimensional, anisotropic potential energy hypersurface, other local minimum structures exist. We have postponed their discussion to this point, because they are not energetically competitive with the global ring structures up to at least $n = 7$ [26,102,109–111], and do not contribute substantially to HF vapor at thermodynamic equilibrium [104] or to the infrared bands observed in low temperature equilibria [18] or in supersonic jet expansions [27,109,110].

Fig. 11 gives a survey over the most important local minima which were found for the HF3BG + SC-2.9 potential energy hypersurface in terms of the energy per monomer required for complete dissociation into HF units. The C_{2v} secondary minimum for $(HF)_3$ has already been discussed in Section 4.5. Its double acceptor motif can be extended to larger clusters,

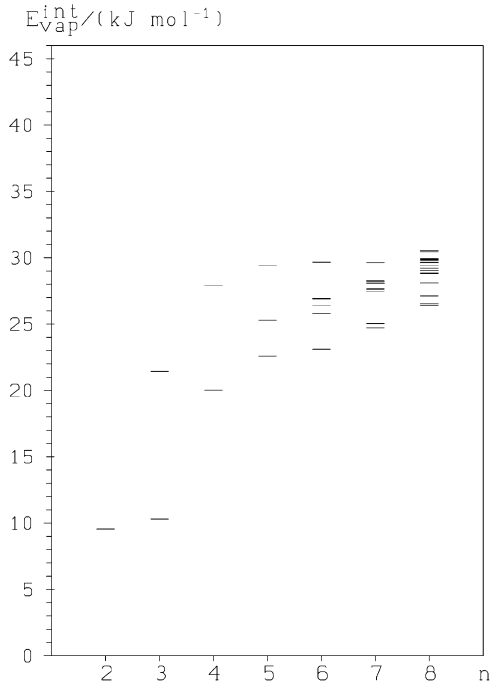

Fig. 11. Integral vaporization energies $E_{vap}^{int}(n)$ for different HF cluster isomers at 0 K corresponding to the process $(1/n)(HF)_n \rightarrow$ HF in the classical approximation for the HF3BG + SC-2.9 potential.

where it leads to structures containing single HF molecules attached to a ring [104]. They account for the second-most stable $(HF)_n$ isomers for $n = 4, 5$, possibly also for $n = 6$. These 'lasso'-type, branched structures [104] have been considered to be thermodynamically or spectroscopically relevant by some authors [38,197]. We cannot confirm this, based on experimental spectra and the HF3BG + SC-2.9 results, also confirmed by DZP + MP2 as well as B3LYP (6-31 + G*) calculations. For example, isomerization of $(HF)_5$ to a tetramer with an attached monomer requires 21, 32, and 34 kJ/mol, respectively, at these levels of theory. Increased ring strain and the loss of cooperative stabilization in the attached HF hydrogen bond account for this effect [31,33,104], and the result predicted by our analytical potential energy surfaces most likely represents a lower bound, since four-body forces are neglected. The same holds for structures with more or longer side chains attached to a ring, which come into play for $n > 5$. Detailed thermodynamic modeling [104,106] including these structures also proves their insignificance at higher temperatures, whereas effective pair potentials can be expected to enhance the branching tendency [38]. The least stable pentamer structure contained in Fig. 11 consists of two ring trimers merged at one of the corners. This structure is also confirmed by quantum-chemical calculations. We note that two recent studies involving model potentials [92,122] come to similar conclusions concerning the isomerism of $(HF)_n$, $n \leq 6$, despite characteristic deficiencies for the smaller clusters and inclusion of some higher than three-body contributions to the potential energy. At these levels, e.g. the ring pentamer is 19 kJ/mol [92] or 27 kJ/mol [122] lower in energy than the tetramer with an attached monomer. In bulky alcohol clusters, lasso structures can compete more easily with simple ring structures, if sterical hindrance and cooperative enhancement cancel each other [195].

Starting with the clusters $(HF)_{7,8}$, isomers built from two sandwiched rings become local minima. In the analytical PES, they even surpass folded ring structures in their stability for $n = 8$. This, however, is most likely an artifact of neglecting 4- and higher-body forces and retaining monomer integrity in the analytical potentials. Ab initio calculations (see Table 2) suggest that the transition to sandwich structures as global minima does not yet happen at $n = 8$. Quite generally, the residual deficiencies of the analytical potential energy surface tend to anticipate structural changes, because they involve a truncation of the mechanisms for simple ring stabilization at the three-body level. Accurate predictions of relative stability in this size range are difficult, because binding *between* saturated hydrogen bonded strands is subtle. We estimate that it contributes around 0.5–2 kJ/mol for a nearest neighbour interaction. A recent investigation of simplified diatomic model potentials [198] also leads to global double ring minima under certain circumstances, indicating the potential importance of this structural element. Double ring structures may play a role in the kinetics of vaporization and nucleation. For example, fragmentation patterns leading to two *oligomer* ring fragments may become energetically competitive with single HF vaporization already for $n = 8$. By combining a clockwise with an anticlockwise ring, chiral structures with interesting racemization paths can be obtained.

While the gas phase of HF is dominated by rings [104], the liquid phase is probably composed mainly of chains [65,93,94,98]. This difference is consistent with the simple Jacobson–Stockmayer model [199] which predicts the ring-to-chain ratio for a given oligomer size to be proportional to the volume or dilution. Binding is expected to remain predominantly one-dimensional in the condensed phase, and this provides a simple qualitative rationalization of the highly associated gas phase and the highly compressible liquid [104]. A washed-out liquid–gas phase transition is regularly found in model simulations of dipolar systems with little dispersive interaction [200], for which HF with its exceptionally low ratio of polarizability to polarity provides a real example. Nevertheless, the detailed structure of 1-D hydrogen bonded liquids such as alcohols and HF remains a difficult challenge [195,201].

5.4. Vibrational dynamics of HF oligomers

Predictions from the present ab initio and analytical potential energy hypersurfaces have been useful in the assignment of HF cluster vibrational spectra [15,27,102,104,105,107,109–111]. The controversy on the assignment of $(HF)_n$ infrared spectra between Refs. [109–111], where the first consistent assignments were obtained for $n = 4$–6, and the more recent Refs. [202,203], where so called size selected techniques were used, has been discussed in detail in Ref. [27] and references given therein. Essentially definitive support for our original assignments [109–111] was provided by a recent, detailed experimental investigation [25]. Since the monomer and pair potentials have been thoroughly tested against experimental dimer results [63], we can concentrate on the effect of neglecting higher than three-body terms in the analytical potentials for larger clusters and on the performance of the harmonic DZP + MP2 results. At DZP + MP2 level, all harmonic dimer frequencies are somewhat overestimated compared to the best estimates [63], but the error is only about 8% for the in-plane intermolecular fundamentals, 4% for the out-of-plane fundamental, and 2% for the intramolecular modes. Therefore, DZP + MP2 results for larger clusters, summarized in Table 3 and Fig. 12, should provide reliable trends of vibrational frequencies with increasing cluster size. Anharmonic contributions to these frequencies are large, but in some cases different contributions may cancel in part [27,110].

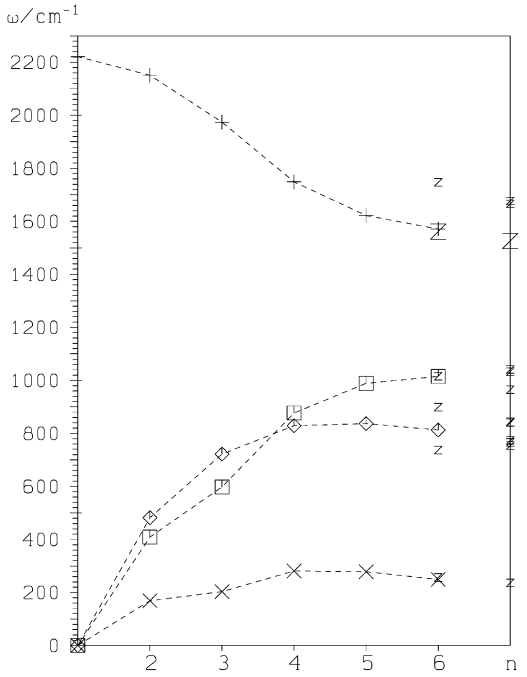

Fig. 12. Harmonic wavenumbers ω/cm^{-1} of $(HF)_n$ IR active vibrations at the DZP + MP2 level as a function of cluster size n. For $n = 2$, the in plane bending and HF stretching frequency pairs are averaged. +: HF stretching ($\omega - 2000\,cm^{-1}$ is plotted); ×: FF stretching; □: in plane bending; ◇: out of plane bending, all for C_{nh} structures; Transitions for the $(HF)_6$ S_6 global minimum and the $(HF)_7$ C_1-symmetry structure are denoted with Z symbols, if they have band strengths in excess of 50 km/mol. Large Z symbols mark the dominant HF stretching bands.

The HF stretching manifold is most sensitive to insufficiencies in the analytical potential parameterization and shows an artificial near-saturation of the harmonic complexation red shifts already for $n > 4$ (see Table 3), whereas the DZP + MP2 results (Table 2 and Fig. 12) and recent spectra of the IR active degenerate stretching fundamentals [109,111,203] indicate that this does not happen for $n < 7$. These insufficiencies are confirmed by the strong dependence of the HF stretching predictions on details of the vibrational coupling. They are in contrast to the *quantitative* success of the analytical potentials in reproducing anharmonic monomer, dimer [62,204] and trimer [106] stretching fundamentals, indicating that neglect of four-body terms dominates the error

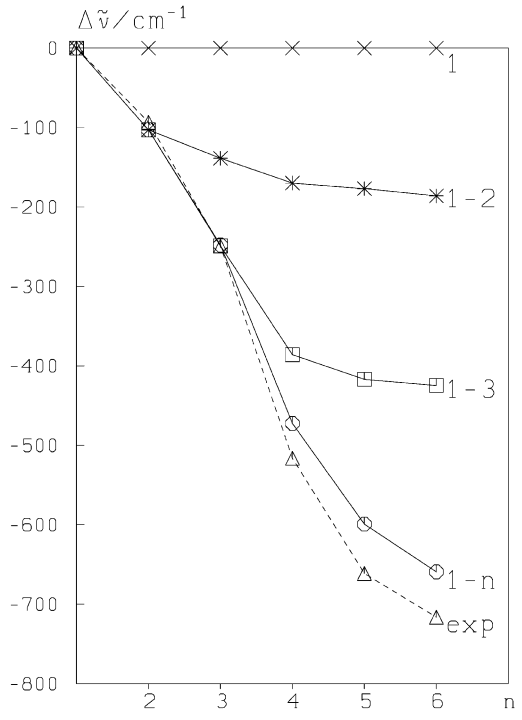

Fig. 13. Harmonic wavenumber shifts $\Delta\tilde{\nu}$ of the IR-active HF stretching fundamental as a function of cluster size including up to one- (1), two- (1–2), three- (1–3) and n-body (1–n) contributions to the total potential energy. Comparison is also made to experimental (exp) anharmonic wavenumber shifts. The harmonic numbers are best estimates based on SC-2.9 + HF3BG and ab initio calculations.

[26]. Fig. 13 shows best estimates of the harmonic HF stretching wavenumber shifts as a function of cluster size, with progressive inclusion of higher-body contributions. A one-body potential, by definition, does not show any cluster size dependence. Two-body contributions induce relatively small shifts, which saturate for $n \approx 4$. Inclusion of 3-body terms leads to accurate predictions for the trimer and sizeable shifts for the larger clusters, but saturation of the shift is already reached for $n \approx 5$. Inclusion of higher than three-body contributions is crucial for the pentamer and larger clusters, as already discussed in Ref. [26]. Compared to these harmonic many-body contributions, total anharmonic effects are relatively small due to cancellation of opposite contributions [27,110], thus explaining why harmonic ab initio predictions can be so useful in the cluster size assignment based on hydride stretching spectra [109]. Among other model potentials including monomer flexibility, a very recent DIIS potential [89] (Table 3) appears to perform somewhat better in the HF stretching domain, since it includes higher than three-body forces in a perturbative manner. On the other hand, an earlier semiempirical treatment [124] fails completely in the prediction of the mode coupling in the HF stretching manifold.

Turning to FF stretching frequencies, preliminary comparison to experimental data is also possible [178]. The broad oligomer absorption observed in long path cell spectra (150–260 cm^{-1} with maximum near 230 cm^{-1}) is undoubtedly due to 'lattice' vibrations in HF clusters ($n > 3$). While these motions are intrinsically weakly IR active, they gain intensity through cooperativity, coupling to librational modes and possibly to the HF stretching dipoles. The latter coupling is strongly promoted by the closeness of hydrogen exchange configurations. The IR active FF stretching frequencies for the cyclic C_{nh} structures go through a maximum between $n = 4$ and $n = 5$ in direct ab initio ($\approx 280\ cm^{-1}$), analytical potential ($\approx 275\ cm^{-1}$) and MMC ($\approx 265\ cm^{-1}$) predictions. This trend is consistent with the stepwise HF vaporization energies. Assuming that off-resonant zero point motional coupling (see Section 4) is the dominating anharmonicity effect also for $n > 3$ and considering that its relative magnitude does not exceed the -20% range found for the trimer, the experimental spectrum [104] is consistent with a *harmonic* wavenumber maximum of about 250–300 cm^{-1}. This agrees well with the DZP + MP2 prediction and is consistent with somewhat underestimated binding energies for the larger clusters in the analytical potentials. Pure pair potentials underestimate the FF stretching frequencies substantially.

In plane degenerate bending frequencies increase steadily from $n = 3$ to $n = 6$ (Fig. 12). The out-of-plane libration is rather constant over the oligomer range studied. This leads to a crossing with the in plane bending wavenumbers between $n = 3$ and $n = 4$ for the analytical, MMC and ab initio potentials. The DIIS model potential does not reproduce this crossing [89], since it underestimates the out-of-plane bending mode by a substantial amount. The

crossing itself can be explained by ring strain, which has more influence on the in plane force constants. Both in- and out-of-plane vibrations give rise to the 10–15 μm band system [104,177], whereas the weaker 8 μm band [104,177] might be due to a combination or overtone transition. The infrared active librational fundamentals have recently been assigned in a jet experiment [24]. They are only 3–7% lower than our harmonic HF3BG + SC-2.9 potential prediction, which itself is somewhat on the low side due to the neglect of 4-body contributions. For the pentamer, experiment [24] is even above the harmonic prediction on the analytical potential energy hypersurface. In contrast, the DZP + MP2 harmonic predictions are systematically above the experimental fundamentals by 12–16%.

Summarizing the vibrational dynamics in HF oligomers, the ab initio results are consistent with the experimental information available, once reasonable anharmonicities are invoked. The analytical predictions reproduce qualitative trends for hydrogen bond modes but there is evidence for a lack of bond strength for $n > 4$, particularly evident in the HF stretching manifold. The true harmonic frequencies are expected in between, closer to the analytical models for $n < 4$ and closer to the ab initio data for $n > 4$. The performance of pure pair potentials is very poor.

Ring puckering will affect the IR selection rules [42], resulting in more than one IR active HF stretching vibration. For the S_6 symmetry predicted at DZP + MP2 level, one half of the fundamentals may be IR active (see Table 3 and Figs. 12 and 14). While the lowest frequency, totally symmetric HF stretching mode remains inactive, the highest frequency non-degenerate mode should become visible as a weak satellite which grows in intensity with increasing puckering extent. At the double harmonic DZP + MP2 level, the satellite band contributes $\approx 5\%$ to the total band strength. Twist- and boat-like distortions lead to more satellite bands. The available IR spectra of $(HF)_6$ [109,197] are too congested to allow for a clear distinction between planar and quasi-planar structures of this complex at the predicted puckering level. A sensitive probe of puckering may also be found in the FIR spectrum below the FF stretching polymer band [178]. While the planar structures have inactive puckering bands and hence do not contribute to spectral congestion, the DZP + MP2 calculations indicate a weakly IR active band near 27 cm^{-1} for the S_6 minimum, which may correspond to a weak broad hump observed in the experimental low temperature cell spectrum [178]. The far infrared promises to be a fruitful spectroscopic region to investigate ring puckering in hydrogen bonded complexes.

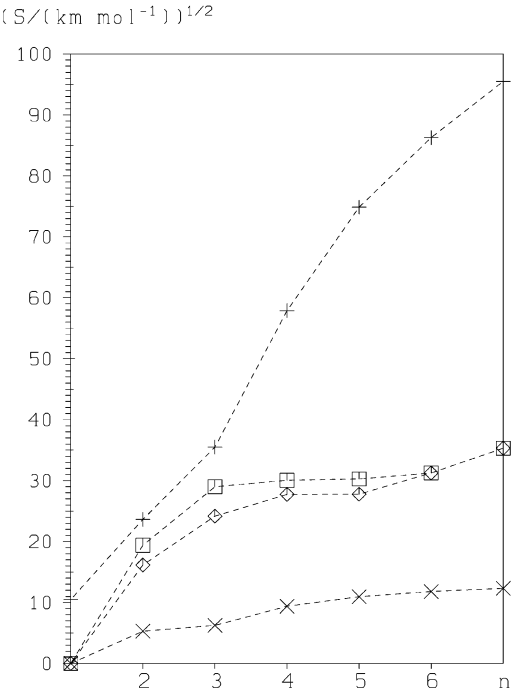

Fig. 14. Square root of C_{nh} $(HF)_n$ DZP + MP2 infrared molar band strengths S in the double-harmonic approximation as a function of cluster size n. Integrated absorption cross sections G, which are directly proportional to squared transition dipole moments, can be obtained with band centers $\tilde{\nu}_0$ via $G \approx S/(\tilde{\nu}_0 N_A)$. We plot S because it allows a direct comparison of predicted IR absorbances for band centers varying over 1–2 orders of magnitude. For the in plane vibrations with $n > 2$, a degeneracy factor of two is included, while for $n = 2$, the corresponding non-degenerate modes (HF stretch and in plane bend) are added together. +: HF stretching; ×: FF stretching; □: in plane bending; ◇: out of plane bending; see Fig. 12 and Table 3 for the corresponding frequencies. The HF stretch intensity increases more than quadratically with cluster size (approximately $\sim n^{2.35\pm0.15}$ up to $n = 6$). The other IR active vibrations grow much more moderately in intensity with increasing cluster size. For the FF stretches, this is in contrast to experimental evidence [178], suggesting anharmonic effects and coupling to the HF modes. The effect of ring strain for $n = 3$ is clearly visible. Also included are band strengths for the C_1 $(HF)_7$ structure.

6. Conclusions

Based on the electronic structure calculations, analytical potential energy hypersurfaces, molecular dynamics results and spectroscopic evidence discussed in the preceding sections, we can draw the following main conclusions:

(i) The three-body contribution to the potential for HF aggregates can be calculated ab initio with relatively high accuracy at little cost. This is in marked contrast to the effort needed for reliable HF pair potentials [63].
(ii) The HF three-body potential makes a very significant contribution to the structure and dynamics of HF oligomers (e.g. $\approx 10\%$ in the hydrogen bond length, $\approx 20\%$ of the binding energy and $\approx 50\%$ of the HF frequency shift in the trimer).
(iii) The ab initio analytical three-body potential (HF3BG) is expected to be accurate (within about 100–200 cm^{-1}) for the $(HF)_3$ configurations relevant to the hydrogen bond dynamics. It is computationally economic and portable between different true pair potentials, although it is of course incompatible with empirical effective HF pair potentials which try to include many-body interactions in an effective way and are therefore of limited use in the description of the HF dimer [65,91,93].
(iv) $(HF)_3$ is the least floppy and most strained of the HF aggregates. Our results for the anharmonic binding energy ($D_0 = 43(3)$ kJ/mol), harmonic frequencies (209, 625, 719, 3884 cm^{-1} for the IR-active vibrations), minimum structure (C_{3h}, $r_{HF} = 93.3(3)$ pm, $R_{FF} = 259(2)$ pm, FFH-angle 24(3)°) and ground state C_0 rotational constant (0.120 cm^{-1} for $(DF)_3$) are among the most reliable predictions for this cluster as derived from an analytically available 12-dimensional potential energy hypersurface. Currently, no need for an empirical refinement of the three-body potential in the hydrogen-bonded region is evident. The interconversion tunneling dynamics is predicted to be complex and slow.
(v) The complete dissociation channel (into three monomer fragments) is probably still open to $(HF)_3$ upon HF stretching excitation in the IR under supersonic jet expansion conditions. Successive deuteration leads to sufficient stabilization to close this channel, leaving dissociation into a dimer and a monomer as the only option. $(DF)_3$ is predicted to be stable for $J = 0$ excitation of *any* vibrational fundamental. This latter prediction relies on anharmonic effects in the zero-point energy and three-body effects in the potential. Neglect of either of these effects in the potential would lead to a predissociative ν_5 fundamental.
(vi) The predictions for higher HF oligomers are limited by the neglect of higher-body contributions to the potential and by the onset of hydrogen exchange. These limitations appear to be acceptably small for many properties of at least the tetramer, the pentamer and the hexamer species. Some predictions, such as harmonic frequencies and absolute binding energies for $n > 3$ are clearly affected by the limitations.
(vii) Voronoi step representation [82] is shown to be a useful tool in the development of multidimensional potential energy surfaces.
(viii) The best estimate for the full anharmonic binding energy of $(HF)_4$ is 84.5 ± 4 kJ/mol [26], suggesting that HF stretching fundamental excitation in the IR is at best *slightly* above threshold for evaporation of one HF unit. More likely, it falls below this threshold. This result is also consistent with a recent ab initio result [24].
(ix) The onset of ring puckering for the global minimum structures of $(HF)_n$ oligomers is located around $n = 6$, but the quantum ground state structure remains quasiplanar and spectroscopic evidence for puckering is currently circumstantial.
(x) Beyond $n = 7$, some indication for stable double ring structures bound to each other via secondary interactions is found. The cluster size beyond which such structures become competitive remains open, as the balance between large single rings and aggregates of smaller rings is very subtle and basis set superposition error becomes a critical issue.

We have described how existing HF pair potential parametrizations can be used in a meaningful way for higher oligomers and in particular for the trimer, by simply adding a three body potential. Many results presented in this work lead to clear predictions for the hydrogen bond structure and dynamics of HF aggregates in general and $(HF)_3$ in particular. Some of these predictions have been tested experimentally [25,27,107,109,197]. The assignment of the very complex $(HF)_n$ cluster infrared spectra in the HF-

stretching fundamental region [15,109–111] was substantially aided by the potentials and quantum chemical calculations presented here. While this assignment has been questioned on the basis of somewhat limited experimental evidence in the past [197, 202,203], it is gratifying to see that our original assignments could be fully confirmed in recent experiments [25]. This provides a nice illustration of the usefulness of such global potentials for the analysis of complex spectra. Another prediction derived from the present potentials concerns the ground state rotational constants and thus microwave spectra observable for the mixed isotopomers $HF(DF)_2$ and $(HF)_2DF$. This is an interesting challenge to experimental rotational spectroscopy [1–5], which we plan to take up in the near future.

The theoretical work in progress or planned concerns the accurate calculation of rovibrational states [205] for $(HF)_3$, and the extension of the potential description to include multidimensional tunneling dynamics with hydrogen exchange [26,27]. Also 4-body and 5-body contributions to the potentials of the higher $(HF)_n$ clusters are being included [26,27]. Finally, a fit of the 3-body dipole moments will provide predictions for absolute intensities of vibrational and rotational transitions of the HF-trimer and its isotopomers.

Acknowledgements

We thank David Luckhaus for substantial help and discussions and Katharina Al-Shamery née von Puttkamer, Ara Apkarian, Andreas Beil, Tucker Carrington Jr, John Farrell, Hans Hollenstein, Brian Howard, Marius Lewerenz, Roberto Marquardt, Alexander Nemukhin, David Nesbitt, Fritz Schaefer, Ulrich Schmitt and Robert O. Watts for discussions and correspondence including various preprints of their work. Our work is supported financially by the Schweizerischer Nationalfonds and the Schweizerischer Schulrat. Grants of computing time on the NEC (CSCS), CRAY (ETH Zürich), IBM and DEC (C^4 project, ETH) computers accessible to us are gratefully acknowledged. We thank B. Löpfe for valuable assistance in using CADPAC on the CRAY.

Appendix A. FORTRAN 77 source code for the analytical HF3BG potential

The FORTRAN 77 subroutine polaris accepts as input the cartesian coordinates *xc* (in bohr) and provides as output *et*, the three-body energy divided by *hc* corresponding to V_{123}^3 in cm^{-1}, Eq. (4).

```
cccccccccccccccccccccccccccccccccccccccccccccccccccccccccccccccccccccccccccccccc
C Supplementary material to ref. [2], given below.
cccccccccccccccccccccccccccccccccccccccccccccccccccccccccccccccccccccccccccccccc
C
C References:
C
C [1] M. Quack, J. Stohner, and M. A. Suhm, J. Molec. Structure 294, 33-36 (1993)
C         "Vibrational dynamics of (HF)_n aggregates from an ab initio based
C         analytical (1+2+3)-body potential"
C
C [2] M. Quack, J. Stohner, and M. A. Suhm, J. Molec. Structure 599, 381-425 (2001)
C         "Analytical three-body interaction potentials and hydrogen bond
C          dynamics of hydrogen fluoride aggregates, (HF)_n, n >= 3"
C
C email:   martin@quack.ch  //  msuhm@gwdg.de
cccccccccccccccccccccccccccccccccccccccccccccccccccccccccccccccccccccccccccccccc
C-----------------------------------------------------------------------------
C             HF3BG Potential
C-----------------------------------------------------------------------------
C subroutine ***polaris(xc,et,p,np)***
C
C xc: cartesian atomic coordinates (bohr)  H1,H2,H3,F1,F2,F3
C et: three body energy/hc in cm-1
C  p: free parameters (p(1)=6e5cm-1, p(2)=1.2e4cm-1, p(3)=0.375e0a0-1,
C                     p(4)=0.88a0-1, p(5)=1.38a0-1)
C np: number of free parameters
C-----------------------------------------------------------------------------
C  Author: M. Suhm
C-----------------------------------------------------------------------------
      subroutine polaris(xc,et,p,np)
C calculation of HF3BG three-body potential model
      implicit double precision (a-h,o-z)
      parameter (n=1)
C number of simultaneous potential evaluations - large values
C give optimum vector processor speedup
      parameter (zero=0.0d0,one=1.0d0,half=0.5d0)
      dimension xc(n,3,6),r(n,3,3),dr(n,3,3,3),rc(n,3,3)
      dimension drc(n,3,3,3),rhh(n,3)
      dimension th(n,3,3),alph(n,3,3),beta(n,3,3),gamma(n,3,3)
      dimension p(*),dmo(n,3),et(n),etb(n,3)
      data apot/5.2d0/apoa/1.5d0/
C polarizability tensor of HF
      data cofa/33972.d0/
```

```
C unit conversion factor (input: bohr, output: cm-1)
      do 10 in=1,n
      et(in)=zero
   10 continue
C no coordinate transformation cartesian--H-F to cartesian--H-COM!
C rhh-i=nonbonded HH
      do 17 in=1,n
      rhh(in,1)=sqrt((xc(in,1,1)-xc(in,1,2))**2+
     *               (xc(in,2,1)-xc(in,2,2))**2+
     *               (xc(in,3,1)-xc(in,3,2))**2)
      rhh(in,2)=sqrt((xc(in,1,1)-xc(in,1,3))**2+
     *               (xc(in,2,1)-xc(in,2,3))**2+
     *               (xc(in,3,1)-xc(in,3,3))**2)
      rhh(in,3)=sqrt((xc(in,1,2)-xc(in,1,3))**2+
     *               (xc(in,2,2)-xc(in,2,3))**2+
     *               (xc(in,3,2)-xc(in,3,3))**2)
   17 continue
      do 18 i=1,3
      do 19 j=1,3
      do 21 in=1,n
      dr(in,1,i,j)=xc(in,1,i)-xc(in,1,j+3)
      dr(in,2,i,j)=xc(in,2,i)-xc(in,2,j+3)
      dr(in,3,i,j)=xc(in,3,i)-xc(in,3,j+3)
C r-ii=bonded H-F
C r-ij=nonbonded H-F
      r(in,i,j)=sqrt(dr(in,1,i,j)**2+dr(in,2,i,j)**2+dr(in,3,i,j)**2)
   21 continue
   19 continue
   18 continue
      do 25 i=1,3
      do 26 in=1,n
      dmo(in,i)=r(in,i,i)/((r(in,i,i)/4.d0)**4+1)
      if(r(in,i,i).gt.2.) then
      dmo(in,i)=dmo(in,i)*exp(-((r(in,i,i)-2.)/2.)**2)
      endif
   26 continue
   25 continue
      do 27 i=1,3
      do 28 j=i+1,3
      do 30 in=1,n
      drc(in,1,i,j)=xc(in,1,j+3)-xc(in,1,i+3)
      drc(in,1,j,i)=-drc(in,1,i,j)
      drc(in,2,i,j)=xc(in,2,j+3)-xc(in,2,i+3)
      drc(in,2,j,i)=-drc(in,2,i,j)
      drc(in,3,i,j)=xc(in,3,j+3)-xc(in,3,i+3)
      drc(in,3,j,i)=-drc(in,3,i,j)
C rc-ij F-F distance
      rc(in,i,j)=sqrt(drc(in,1,i,j)**2+drc(in,2,i,j)**2
     *                +drc(in,3,i,j)**2)
      rc(in,j,i)=rc(in,i,j)
   30 continue
   28 continue
   27 continue
      do 34 i=1,3
      do 35 j=i+1,3
      k=6-i-j
      do 37 in=1,n
      alph(in,i,j)=((dr(in,1,i,i)*dr(in,1,j,j)+
     *               dr(in,2,i,i)*dr(in,2,j,j)+
     *               dr(in,3,i,i)*dr(in,3,j,j))/
     *               (r(in,i,i)*r(in,j,j)))
      alph(in,j,i)=alph(in,i,j)
      beta(in,j,i)=((drc(in,1,i,k)*drc(in,1,j,k)+
     *               drc(in,2,i,k)*drc(in,2,j,k)+
     *               drc(in,3,i,k)*drc(in,3,j,k))/
     *               (rc(in,i,k)*rc(in,j,k)))
      beta(in,i,j)=beta(in,j,i)
   37 continue
   35 continue
   34 continue
      do 38 i=1,3
      do 39 j=1,3
      if(i.ne.j)then
      k=6-i-j
      do 41 in=1,n
```

```
   gamma(in,i,j)=((dr(in,1,k,k)*drc(in,1,i,j)+
  *                dr(in,2,k,k)*drc(in,2,i,j)+
  *                dr(in,3,k,k)*drc(in,3,i,j))/
  *                (r(in,k,k)*rc(in,i,j)))
   th(in,i,j)=((dr(in,1,i,i)*drc(in,1,i,j)+
  *             dr(in,2,i,i)*drc(in,2,i,j)+
  *             dr(in,3,i,i)*drc(in,3,i,j))/
  *             (r(in,i,i)*rc(in,i,j)))
41 continue
   endif
39 continue
38 continue

   do 42 i=1,3
   do 43 k=i+1,3
   j=6-i-k
   do 45 in=1,n
   etb(in,j)=-((alph(in,i,k)
  *          -3*gamma(in,i,j)*th(in,i,j)
  *          -3*gamma(in,k,j)*th(in,k,j)+
  *          9*beta(in,k,i)*th(in,i,j)*th(in,k,j))
  *          *apot+
  *          (alph(in,i,j)+3*th(in,i,j)*th(in,j,i))*
  *          (alph(in,k,j)+3*th(in,k,j)*th(in,j,k))
  *          *apoa)*
  *          1.2321d0*dmo(in,i)*dmo(in,k)*cofa/
  *         (((rc(in,i,j))**3)*((rc(in,k,j))**3))
   et(in)=et(in)+etb(in,j)
45 continue
43 continue
42 continue
   do 46 in=1,n
   et(in)=et(in)+p(1)*(
  *         -9*(
  *          exp(-p(5)*(r(in,1,2)+r(in,2,3)))
  *         +exp(-p(5)*(r(in,1,3)+r(in,2,1)))
  *         +exp(-p(5)*(r(in,2,3)+r(in,3,1)))
  *         +exp(-p(5)*(r(in,2,1)+r(in,3,2)))
  *         +exp(-p(5)*(r(in,1,2)+r(in,3,1)))
  *         +exp(-p(5)*(r(in,1,3)+r(in,3,2)))
  *         )+
  *         2*(
  *          exp(-2*p(3)*(r(in,1,3)+r(in,2,3)+rhh(in,1)))
  *         +exp(-2*p(3)*(r(in,1,2)+r(in,3,2)+rhh(in,2)))
  *         +exp(-2*p(3)*(r(in,2,1)+r(in,3,1)+rhh(in,3)))
  *         )+
  *         90*(
  *          exp(-4*p(3)*(r(in,1,3)+r(in,2,1)+r(in,1,1)))
  *         +exp(-4*p(3)*(r(in,1,2)+r(in,3,1)+r(in,1,1)))
  *         +exp(-4*p(3)*(r(in,2,1)+r(in,3,2)+r(in,2,2)))
  *         +exp(-4*p(3)*(r(in,2,3)+r(in,1,2)+r(in,2,2)))
  *         +exp(-4*p(3)*(r(in,3,2)+r(in,1,3)+r(in,3,3)))
  *         +exp(-4*p(3)*(r(in,3,1)+r(in,2,3)+r(in,3,3)))
  *         )+
  *         60*(
  *          exp(-4*p(3)*(r(in,1,2)+r(in,2,3)+r(in,1,1)))
  *         +exp(-4*p(3)*(r(in,1,3)+r(in,3,2)+r(in,1,1)))
  *         +exp(-4*p(3)*(r(in,2,1)+r(in,1,3)+r(in,2,2)))
  *         +exp(-4*p(3)*(r(in,2,3)+r(in,3,1)+r(in,2,2)))
  *         +exp(-4*p(3)*(r(in,3,2)+r(in,2,1)+r(in,3,3)))
  *         +exp(-4*p(3)*(r(in,3,1)+r(in,1,2)+r(in,3,3)))
  *         )
  *         -3*(
  *         exp(-2*p(3)*(r(in,1,2)+r(in,2,3)+r(in,3,1)))
  *         +exp(-2*p(3)*(r(in,1,3)+r(in,2,1)+r(in,3,2)))
  *         )
  *         -2*(
  *         exp(-p(4)*(rhh(in,2)+rhh(in,3)+rhh(in,1)))
  *         )+
  *         8*(
  *         exp(-p(3)*(r(in,1,2)+r(in,2,3)+r(in,3,1)
  *         +r(in,1,3)+r(in,2,1)+r(in,3,2)))
  *         )
  *         )
   if(et(in).ge.p(2)) et(in)=p(2)-one
   et(in)=-et(in)/(et(in)/p(2)-1.d0)
46 continue
   return
   end
```

References

[1] A. Bauder, in: R. Fausto (Ed.), Low Temperature Molecular Spectroscopy, Kluwer Academic Publishers, Dordrecht, 1996, p. 271.
[2] A. Bauder, in: R. Fausto (Ed.), Low Temperature Molecular Spectroscopy, Kluwer Academic Publishers, Dordrecht, 1996, p. 291.
[3] A. Bauder, J. Mol. Struct. 408/409 (1997) 33–37.
[4] T. Brupbacher, J. Makarewicz, A. Bauder, J. Chem. Phys. 108 (1998) 3932–3939.
[5] D. Priem, T.-K. Ha, A. Bauder, J. Chem. Phys. 113 (2000) 169–175.
[6] T.R. Dyke, B.J. Howard, W. Klemperer, J. Chem. Phys. 56 (1972) 2442–2454.
[7] A.S. Pine, J. Mol. Spectrosc. 82 (1980) 435–448.
[8] A.S. Pine, W.J. Lafferty, J. Chem. Phys. 78 (1983) 2154–2162.
[9] A.S. Pine, W.J. Lafferty, B.J. Howard, J. Chem. Phys. 81 (1984) 2939–2950.
[10] A.S. Pine, A. Fried, J.W. Elkins, J. Mol. Spectrosc. 109 (1985) 30–45.
[11] R.E. Miller, Acc. Chem. Res. 23 (1990) 10–16.
[12] B.J. Howard, Farad. Discuss. Chem. Soc. 71 (1981) 23–29.
[13] K.v. Puttkamer, M. Quack, Mol. Phys. 62 (1987) 1047–1064.
[14] K.v. Puttkamer, M. Quack, M.A. Suhm, Mol. Phys. 65 (1988) 1025–1045.
[15] K.v. Puttkamer, M. Quack, M.A. Suhm, Infrared Phys. 29 (1989) 535–539.
[16] M. Quack, M.A. Suhm, Chem. Phys. Lett. 171 (1990) 517–524.
[17] H. Hollenstein, M. Quack, to be published.
[18] K.v. Puttkamer, M. Quack, Chem. Phys. 139 (1989) 31–53.
[19] M.A. Suhm, J.T. Farrell Jr., A. McIlroy, D.J. Nesbitt, J. Chem. Phys. 97 (1992) 5341–5354.
[20] H.-C. Chang, W. Klemperer, J. Chem. Phys. 98 (1993) 2497–2506.
[21] H.-C. Chang, F.-M. Tao, W. Klemperer, J. Chem. Phys. 99 (1993) 9337–9349.
[22] Y. He, H.B. Müller, M. Quack, M.A. Suhm, to be published.
[23] R. Signorell, Y. He, H.B. Müller, M. Quack, M.A. Suhm, in: J.P. Maier, M. Quack (Eds.), Proceedings of the 10th International Symposium on Atomic, Molecular, Cluster, Ion and Surface Physics, VdF Publishers, Zürich, 1996, pp. 256–259.
[24] T.A. Blake, S.W. Sharpe, S.S. Xantheas, J. Chem. Phys. 113 (2000) 707–718.
[25] L. Oudejans, R.E. Miller, J. Chem. Phys. 113 (2000) 971–978.
[26] M. Quack, M.A. Suhm, Potential energy hypersurfaces for hydrogen bonded clusters $(HF)_n$, in: J.-L. Calais, E.S. Kryachki (Eds.), Conceptual Perspectives in Quantum Chemistry, Conceptual Trends in Quantum Chemistry, vol. III, Kluwer Academic Publishers, Dordrecht, 1997, pp. 415–463.
[27] M. Quack, M.A. Suhm, Spectroscopy and quantum dynamics of hydrogen fluoride clusters, in: J. Bowman, Z. Bačić (Eds.), Advances in molecular Vibrations and Collision Dynamics, Molecular Clusters, vol. III, JAI Press, 1998, pp. 205–248.
[28] H.S. Frank, W.-Y. Wen, Discuss. Farad. Soc. 24 (1957) 133–140.
[29] L. Jansen, in: P.-O. Löwdin (Ed.), Advances in Quantum Chemistry, vol. 2, Academic Press, New York, 1965, pp. 119–194.
[30] K.F. Niebel, J.A. Venables, in: M.L. Klein, J.A. Venables (Eds.), Rare Gas Solids, vol. 1, Academic Press, London, 1976, pp. 558–589.
[31] D. Hankins, J.W. Moskowitz, F.H. Stillinger, Chem. Phys. Lett. 4 (1970) 527–530.
[32] P. Kollman, J. Am. Chem. Soc. 99 (1977) 4875–4894.
[33] P. Schuster, A. Karpfen, A. Beyer, Cooperative phenomena in molecular systems, in: H. Ratajczak, W.J. Orville-Thomas (Eds.), Molecular Interactions, Wiley, New York, 1980, pp. 117–149 chap. 5.
[34] P. Schuster, Angew. Chem. Int. Ed. Engl. 20 (1981) 546–568.
[35] K.D. Kolenbrander, C.E. Dykstra, J.M. Lisy, J. Chem. Phys. 88 (1988) 5995–6012.
[36] V. Mohan, J.B. Anderson, J. Chem. Phys. 92 (1990) 6971–6973.
[37] J.M. Hutson, J.A. Beswick, N. Halberstadt, J. Chem. Phys. 3 (1989) 1337–1344.
[38] H. Sun, R.O. Watts, U. Buck, J. Chem. Phys. 96 (1992) 1810–1821.
[39] F. Huisken, Adv. Chem. Phys. 81 (1992) 63–140.
[40] O. Mó, M. Yáñez, J. Elguero, J. Chem. Phys. 97 (1992) 6628–6638.
[41] A.R. Cooper, J.M. Hutson, J. Chem. Phys. 98 (1993) 5337–5351.
[42] U. Buck, B. Schmidt, J. Chem. Phys. 98 (1993) 9410–9424.
[43] B.J. Mhin, J. Kim, S. Lee, J.Y. Lee, K.S. Kim, J. Chem. Phys. 100 (1994) 4484–4486.
[44] J. Han, Z. Wang, A.L. McIntosh, R.R. Lucchese, J.W. Bevan, J. Chem. Phys. 100 (1994) 7101–7108.
[45] M.J. Elrod, R.J. Saykally, Chem. Rev. 94 (1994) 1975–1997.
[46] I.G. Kaplan, R. Santamaria, O. Novaro, J. Mol. Spectrosc. 84 (1994) 105–114.
[47] J.K. Gregory, D.C. Clary, J. Chem. Phys. 103 (1995) 8924–8930.
[48] U. Buck, I. Ettischer, M. Melzer, V. Buch, J. Sadlej, Phys. Rev. Lett. 80 (1998) 2578–2581.
[49] B.M. Axilrod, E. Teller, J. Chem. Phys. 11 (1943) 299–300.
[50] D.G. Bounds, A. Hinchliffe, Mol. Phys. 40 (1980) 989–996.
[51] P. Cieplak, T.P. Lybrand, P.A. Kollman, J. Chem. Phys. 86 (1987) 6393–6403.
[52] J.E. Combariza, N.R. Kestner, J. Jortner, Chem. Phys. Lett. 203 (1993) 423–428.
[53] E. Clementi, W. Kolos, G.C. Lie, G. Ranghino, Int. J. Quant. Chem. 17 (1980) 377–398.
[54] H. Saint-Martin, C. Medina-Llanos, I. Ortega-Blake, J. Chem. Phys. 93 (1990) 6448–6452.
[55] Y. Hannachi, B. Silvi, Y. Bouteiller, J. Chem. Phys. 97 (1992) 1911–1918.
[56] J.G.C.M.v. Duijneveldt-van de Rijdt, F.B.v. Duijneveldt, Chem. Phys. 175 (1993) 271–281.
[57] K. Laasonen, M. Sprik, M. Parrinello, R. Car, J. Chem. Phys. 99 (1993) 9080–9089.

[58] H. Guo, M. Karplus, J. Phys. Chem. 98 (1994) 7104–7105.
[59] M. Kofranek, H. Lischka, A. Karpfen, Chem. Phys. 121 (1988) 137–153.
[60] P.R. Bunker, P. Jensen, A. Karpfen, M. Kofranek, H. Lischka, J. Chem. Phys. 92 (1990) 7432–7440.
[61] M. Quack, M.A. Suhm, J. Chem. Phys. 95 (1991) 28–59.
[62] D. Luckhaus, R. Meyer, M. Quack, M.A. Suhm, Quasilbound dynamics of $(HF)_2$: an adiabatic model. To be published.
[63] W. Klopper, M. Quack, M.A. Suhm, J. Chem. Phys. 108 (1998) 10096–10115.
[64] M. Quack, M.A. Suhm, Mol. Phys. 69 (1990) 791–801.
[65] M.E. Cournoyer, W.L. Jorgensen, Mol. Phys. 51 (1984) 119–132.
[66] H.J.C. Berendsen, J.R. Grigera, T.P. Straatsma, J. Phys. Chem. 91 (1987) 6269–6271.
[67] W.F. van Gunsteren, H.J.C. Berendsen, Angew. Chem. Int. Ed. Engl. 29 (1990) 992–1023.
[68] O. Steinhauser, S. Boresch, H. Bertagnolli, Mol. Simulation 7 (1991) 71–88.
[69] J.K. Gregory, D.C. Clary, K. Liu, M.G. Brown, R.J. Saykally, Science 275 (1997) 814–817.
[70] B. Hartke, M. Schütz, H.-J. Werner, Chem. Phys. 239 (1998) 561–572.
[71] C. Votava, R. Ahlrichs, A. Geiger, J. Chem. Phys. 78 (1983) 6841–6848.
[72] S.A.C. McDowell, C.R. LeSueur, A.D. Buckingham, A.J. Stone, Mol. Phys. 77 (1992) 823–835.
[73] M.M. Szczęśniak, G. Chałasiński, J. Mol. Struct. (Theochem) 261 (1992) 37–54.
[74] E. Clementi, G. Corongiu, Int. J. Quantum. Chem. (Quant. Biol. Symp.) 10 (1983) 31–41.
[75] U. Niesar, G. Corongiu, M.-J. Huang, M. Dupuis, E. Clementi, Int. J. Quant. Chem. (Symp.) 23 (1989) 421–443.
[76] S.S. Xantheas, J. Chem. Phys. 100 (1994) 7523–7534.
[77] A.J. Stone, The Theory of Intermolecular Forces, Clarendon Press, Oxford, 1996.
[78] G. Chałasiński, S.M. Cybulski, M.M. Szczęśniak, S. Scheiner, J. Chem. Phys. 91 (1989) 7048–7056.
[79] Z. Latajka, S. Scheiner, Chem. Phys. 122 (1988) 413–430.
[80] G. Chałasiński, M.M. Szczęśniak, Chem. Rev. 94 (1994) 1723–1765.
[81] G.S. Tschumper, Y. Yamaguchi, H.F. Schaefer III, J. Chem. Phys. 106 (1997) 9627–9633.
[82] M.A. Suhm, Chem. Phys. Lett. 214 (1993) 373–380.
[83] M.A. Suhm, Chem. Phys. Lett. 223 (1994) 474–480.
[84] A. Beyer, A. Karpfen, P. Schuster, Chem. Phys. Lett. 67 (1979) 369–373.
[85] A. Karpfen, A. Beyer, P. Schuster, Chem. Phys. Lett. 102 (1983) 289–291.
[86] J.F. Gaw, Y. Yamaguchi, M.A. Vincent, H.F. Schaefer III, J. Am. Chem. Soc. 106 (1984) 3133–3138.
[87] S. Liu, D.W. Michael, C.E. Dykstra, J.M. Lisy, J. Chem. Phys. 84 (1986) 5032–5036.
[88] A. Karpfen, Int. J. Quant. Chem. (Quant. Chem. Symp.) 24 (1990) 129–140.
[89] M. Ovchinnikov, V.A. Apkarian, J. Chem. Phys. 110 (1999) 9842–9852.
[90] C.E. Dykstra, Chem. Phys. Lett. 141 (1987) 159–162.
[91] C. Zhang, D.L. Freeman, J.D. Doll, J. Chem. Phys. 91 (1989) 2489–2497.
[92] M.P. Hodges, A.J. Stone, E.C. Lago, J. Phys. Chem. A 102 (1998) 2455–2465.
[93] M.L. Klein, I.R. McDonald, J. Chem. Phys. 71 (1979) 298–308.
[94] M. Deraman, J.C. Dore, J.G. Powles, J.H. Holloway, P. Chieux, Mol. Phys. 55 (1985) 1351–1367.
[95] P. Otto, E.O. Steinborn, Solid State Commun. 58 (1986) 281–284.
[96] M. Springborg, Phys. Rev. B 38 (1988) 1483–1503.
[97] M. Springborg, Int. Rev. Phys. Chem. 12 (1993) 241–303.
[98] U. Röthlisberger, M. Parrinello, J. Chem. Phys. 106 (1997) 4658–4664.
[99] N. Karger, H.-D. Lüdemann, J. Chem. Phys. 109 (1998) 3301–3303.
[100] D.P. Visco Jr, D.A. Kofke, J. Chem. Phys. 109 (1998) 4015–4027.
[101] T. Pfleiderer, I. Waldner, H. Bertagnolli, K. Tödheide, H.E. Fischer, J. Chem. Phys. 113 (2000) 3690–3696.
[102] M. Quack, J. Stohner, M.A. Suhm, J. Mol. Struct. 294 (1993) 33–36.
[103] M.A. Suhm, D.J. Nesbitt, Chem. Soc. Rev. 24 (1995) 45–54.
[104] M.A. Suhm, Ber. Bunsenges. Phys. Chem. 99 (1995) 1159–1167.
[105] C. Maerker, P. von Ragué Schleyer, K.R. Liedl, T.-K. Ha, M. Quack, M.A. Suhm, J. Comput. Chem. 18 (1997) 1695–1719.
[106] M.A. Suhm, HF Dampf. Habilitationsschrift, ETH Zürich 1995 (1995) a postscript file of this thesis is available upon request from the author.
[107] M.A. Suhm, J.T. Farrell Jr., S. Ashworth, D.J. Nesbitt, J. Chem. Phys. 98 (1993) 5985–5989.
[108] D.J. Nesbitt, in: J. Jortner, R.D. Levine, B. Pullman (Eds.), Reaction Dynamics in Clusters and Condensed Phases, vol. 26, Kluwer Academic Publishers, Dordrecht, 1994, pp. 137–151.
[109] M. Quack, U. Schmitt, M.A. Suhm, Chem. Phys. Lett. 208 (1993) 446–452.
[110] D. Luckhaus, M. Quack, U. Schmitt, M.A. Suhm, Ber. Bunsenges. Phys. Chem. 99 (1995) 457–468.
[111] M. Quack, U. Schmitt, M.A. Suhm, Chem. Phys. Lett. 269 (1997) 29–38.
[112] J.N. Murrell, S. Carter, S.C. Farantos, P. Huxley, A.J.C. Varandas, Potential Energy Functions, Wiley, New York, 1984.
[113] A.J.C. Varandas, R.F. Nalewajski, Chem. Phys. Lett. 205 (1993) 253–259.
[114] S.F. Boys, F. Bernardi, Mol. Phys. 19 (1970) 553–566.
[115] R.D. Amos, J.E. Rice, The Cambridge Analytical Derivatives Package, Issue 4.2, 1990.
[116] M.J. Frisch, G.W. Trucks, M. Head-Gordon, P.M.W. Gill, M.W. Wong, J.B. Foresman, B.G. Johnson, H.B. Schlegel, M.A. Robb, E.S. Replogle, R. Gomperts, J.L. Andres, K. Raghavachari, J.S. Binkley, C. Gonzales, R.L. Martin, D.J. Fox, D.J. Defrees, J. Baker, J.P. Stewart, J.A. Pople,

GAUSSIAN 92, Revision F.4. Gaussian Inc., Pittsburgh PA, 1992.
[117] S. Huzinaga, J. Chem. Phys. 42 (1965) 1293–1302.
[118] T.H. Dunning Jr, J. Chem. Phys. 55 (1971) 716–723.
[119] W. Klopper, M. Quack, M.A. Suhm, Mol. Phys. 94 (1998) 105–119.
[120] I. Mayer, P.R. Surjan, Chem. Phys. Lett. 191 (1992) 497–499.
[121] C.E. Dykstra, J. Phys. Chem. 94 (1990) 180–185.
[122] B.L. Grigorenko, A.A. Moskovsky, A.V. Nemukhin, J. Chem. Phys. 111 (1999) 4442–4452.
[123] W.D. Chandler, K.E. Johnson, J.L.E. Campbell, Inorg. Chem. 34 (1995) 4943–4949.
[124] G.V. Yukhnevich, E.G. Tarakanova, A.V. Nemukhin, Russ. Chem. Bull. 46 (1997) 414–422.
[125] M.A. Suhm, R.O. Watts, Phys. Rep. 204 (1991) 293–329.
[126] M.A. Suhm, R.O. Watts, Mol. Phys. 73 (1991) 463–469.
[127] M. Quack, Mol. Phys. 34 (1977) 477–504.
[128] A.J. Perkins, J. Phys. Chem. 68 (1964) 654–655.
[129] J.S. Muenter, J. Chem. Phys. 56 (1972) 5409–5412.
[130] O. Christiansen, C. Hättig, J. Gauss, J. Chem. Phys. 109 (1998) 4745–4757.
[131] W.T. Zemke, W.C. Stwalley, S.R. Langhoff, G.L. Valderrama, M.J. Berry, J. Chem. Phys. 95 (1991) 7846–7853.
[132] W.A. Lester Jr, B.L. Hammond, Ann. Rev. Phys. Chem. 41 (1990) 283–311.
[133] J.B. Anderson, J. Chem. Phys. 65 (1976) 4121–4127.
[134] A. Lüchow, J.B. Anderson, Ann. Rev. Phys. Chem. 51 (2000) 501–526.
[135] D. Ceperley, B. Alder, Science 231 (1986) 555–560.
[136] P.J. Reynolds, J. Tobochnik, H. Gould, Computers in Physics 4 (1990) 662–668.
[137] R. Toral, A. Chakrabarti, Comput. Phys. Commun. 74 (1993) 327–334.
[138] R. Bianchi, D. Bressanini, P. Cremaschi, G. Morosi, Comput. Phys. Commun. 74 (1993) 153–163.
[139] D.F. Coker, R.E. Miller, R.O. Watts, J. Chem. Phys. 82 (1985) 3554–3562.
[140] V. Buch, J. Chem. Phys. 97 (1992) 726–729.
[141] M. Lewerenz, R.O. Watts, Mol. Phys. 81 (1994) 1075–1091.
[142] M. Caffarel, P. Claverie, C. Mijoule, J. Andzelm, D.R. Salahub, J. Chem. Phys. 90 (1989) 990–1002.
[143] M. Quack, J. Troe, Ber. Bunsenges. Phys. Chem. 78 (1974) 240–252.
[144] M. Quack, J. Troe, Statistical adiabatic channel model, in: P.v. Ragué Schleyer, N. Allinger, T. Clark, J. Gasteiger, P.A. Kollman, H.F. Schaefer III, P.R. Schreiner (Eds.), Encyclopedia of Computational Chemistry, vol. 4, Wiley, New York, 1998, pp. 2708–2726.
[145] M. Quack, M.A. Suhm, Chem. Phys. Lett. 183 (1991) 187–194.
[146] B. Fehrensen, D. Luckhaus, M. Quack, Z. Phys. Chem. N.F. 209 (1999) 1–19.
[147] B. Fehrensen, D. Luckhaus, M. Quack, Chem. Phys. Lett. 300 (1999) 312–320.
[148] P.E. Cade, W.M. Huo, J. Chem. Phys. 47 (1967) 614–672.
[149] S. Peyerimhoff, Z.f. Naturforschung A 18 (1963) 1197–1204.
[150] V. Bondybey, P.K. Pearson, H.F. Schaefer III, J. Chem. Phys. 57 (1972) 1123–1128.
[151] H. Müller, R. Franke, R. Jaquet, W. Kutzelnigg, Theor. Chem. Acc. 100 (1998) 85–102.
[152] M. Quack, Annu. Rev. Phys. Chem. 41 (1990) 839–874.
[153] R. Mecke, Z. Physik 81 (1933) 313–331.
[154] G. Herzberg, Molecular Spectra and Molecula Structure. II. Infrared and Raman Spectra of Polyatomic Molecules, D. van Nostrand, New York, 1945.
[155] D. Lukhaus, M. Quack, Mol. Phys. 68 (1989) 745–758.
[156] D.R. Herschbach, V.W. Laurie, J. Chem. Phys. 37 (1962) 1668–1686.
[157] J.K.G. Watson, J. Chem. Phys. 98 (1993) 5302–5309.
[158] H. Hollenstein, R.R. Marquardt, M. Quack, M.A. Suhm, J. Chem. Phys. 101 (1994) 3588–3602.
[159] C. Eckart, Phys. Rev. 47 (1935) 552–558.
[160] P. Sandler, V. Buch, D.C. Clary, J. Chem. Phys. 101 (1994) 6353–6355.
[161] H.-S. Lee, J.M. Herbert, A.B. McCoy, J. Chem. Phys. 110 (1999) 5481–5484.
[162] M.P. Allen, D.J. Tildesley, Computer Simulation of Liquids, Clarendon Press, Oxford, 1989.
[163] C. Tsoo, C.L. Brooks III, J. Chem. Phys. 101 (1994) 6405–6411.
[164] H.E. Scheraga, Predicting three-dimensional structures of oligopeptides, in: K.B. Lipkowitz, D.B. Boyd (Eds.), Reviews in Computational Chemistry, vol. 3, VCH, Wienhiem, 1992, pp. 73–142 chap. 2.
[165] K.A. Olszewski, L. Piela, H.A. Scheraga, J. Phys. Chem. 96 (1992) 4672–4676.
[166] R.L. Somorjai, J. Phys. Chem. 95 (1991) 4141–4146.
[167] P. Amara, D. Hsu, J.E. Straub, J. Phys. Chem. 97 (1993) 6715–6721.
[168] A.B. Finnila, M.A. Gomez, C. Sebenik, C. Stenson, J.D. Doll, Chem. Phys. Lett. 219 (1994) 343–348.
[169] G. Voronoï, J. reine, Angew. Math. 134 (1908) 199–287.
[170] A. Okabe, B. Boots, K. Sugihara, Spatial Tesselations, Concepts and Applications of Voronoi Diagrams, Wiley, Chichester, 1992.
[171] D.W. Michael, J.M. Lisy, J. Chem. Phys. 85 (1986) 2528–2537.
[172] E.J. Bohac, M.D. Marshall, R.E. Miller, J. Chem. Phys. 96 (1992) 6681–6695.
[173] D.J. Nesbitt, Chem. Rev. 88 (1988) 843–870.
[174] T.H. Osterheld, J.I. Brauman, J. Am. Chem. Soc. 114 (1992) 7158–7164.
[175] L. Andrews, Applications of FT-IR spectroscopy, in: J.R. Durig (Ed.), Vibrational Spectra and Structure, vol. 18, Elsevier, Amsterdam, 1990, pp. 183–216.
[176] L. Andrews, S.R. Davis, R.D. Hunt, Mol. Phys. 77 (1992) 993–1003.
[177] D.F. Smith, J. Chem. Phys. 28 (1958) 1040–1056.
[178] M. Quack, M.A. Suhm, Chem. Phys. Lett. 171 (1990) 517–524.
[179] D.H. Zhang, Q. Wu, J.Z.H. Zhang, M. von Dirke, Z. Bačić, J. Chem. Phys. 102 (1995) 2315–2325.

[180] K. Honda, K. Kitaura, K. Nishimoto, Bull. Chem. Soc. Japan 65 (1992) 3122–3134.
[181] P. Groner, Spectrochim. Acta A 49 (1993) 1935–1946.
[182] M. Quack, Phil. Trans. R. Soc. Lond. A 332 (1990) 203–220.
[183] A.D. Buckingham, L. Fan-Chen, Int. Rev. Phys. Chem. 1 (1981) 253–269.
[184] A.C. Legon, D.J. Millen, Chem. Phys. Lett. 147 (1988) 484–489.
[185] E.U. Franck, F. Meyer, Z. Elektrochemie 63 (1959) 571–582.
[186] J. Janzen, L.S. Bartell, J. Chem. Phys. 50 (1969) 3611–3618.
[187] Y.-T. Chang, W.H. Miller, J. Phys. Chem. 94 (1990) 5884–5888.
[188] A. Banerjee, N. Adams, J. Simons, R. Shepard, J. Phys. Chem. 89 (1985) 52–57.
[189] J.D. Dunitz, J. Waser, J. Am. Chem. Soc. 94 (1972) 5645–5650.
[190] A. Karpfen, O. Yanovitskii, J. Mol. Struct. (Theochem) 307 (1994) 81–97.
[191] Gmelin Handbook of Inorganic Chemistry; Fluorine, Springer, Berlin, vol. 5, 1926, pp. 33–37.
[192] Gmelin Handbook of Inorganic Chemistry; Fluorine, Springer, Berlin, Suppl. vol. 1, 1959, pp. 142–181.
[193] Gmelin Handbook of Inorganic Chemistry; Fluorine, Springer, Berlin, Suppl. vol. 3, 1982, pp. 1–119.
[194] L.A. Curtiss, M. Blander, Chem. Rev. 88 (1988) 827–841.
[195] D. Zimmermann, T. Häber, H. Schaal, M.A. Suhm, Mol. Phys. 99 (2001) 413–426.
[196] T. Häber, U. Schmitt, M.A. Suhm, Phys. Chem. Chem. Phys. 1 (1999) 5573–5582.
[197] F. Huisken, E.G. Tarakanova, A.A. Vigasin, G.V. Yukhnevich, Chem. Phys. Lett. 245 (1995) 319–325.
[198] A.S. Clarke, G.N. Patey, J. Chem. Phys. 100 (1994) 2213–2219.
[199] H. Jacobson, W.H. Stockmayer, J. Chem. Phys. 18 (1950) 1600–1606.
[200] M.E. van Leeuwen, B. Smit, Phys. Rev. Lett. 71 (1993) 3991–3994.
[201] F. Weinhold, J. Chem. Phys. 109 (1998) 367–372.
[202] F. Huisken, M. Kaloudis, A. Kulcke, D. Voelkel, Infrared Phys. Technol. 36 (1995) 171–178.
[203] F. Huisken, M. Kaloudis, A. Kulcke, C. Laush, J.M. Lisy, J. Chem. Phys. 103 (1995) 5366–5377.
[204] Z. Bacic, Y. Qi, J.Z.H. Zhang, H. Müller, M. Quack, to be published; J. Blumberger, L. Oeltjen, M. Quack, Z. Bacic and Y. Qiu, Faraday Disc. Chem. Soc. (2001), in press; and to be published.
[205] X. Wang, T. Carrington Jr, Can. J. Phys. (2001).